KSME

Springer

Journal of Mechanical Science and Technology 37 (2) 2023

Original Article
DOI 10.1007/s12206-023-0134-1

Keywords:
· Parallel manipulator
· Kinematics model
· Principle of virtual work
· Inverse dynamics

Correspondence to:
Hongbo Wang
hongbo_w@ysu.edu.cn

Citation:
Zhang, X., Wang, H., Rong, Y., Niu, J., Tian, J., Li, S., Ning, Y. (2023). Improved inverse kinematics and dynamics model research of general parallel mechanisms. Journal of Mechanical Science and Technology 37 (2) (2023) 943~954.
http://doi.org/10.1007/s12206-023-0134-1

Received April 9th, 2022
Revised September 24th, 2022
Accepted October 10th, 2022

† Recommended by Editor Ja Choon Koo

Improved inverse kinematics and dynamics model research of general parallel mechanisms

Xingchao Zhang[1,2], Hongbo Wang[1,3], Yu Rong[4], Jianye Niu[1,2], Junjie Tian[1,2], Shanshan Li[1,2] and Yuansheng Ning[1,2]

[1]Hebei Provincial Key Laboratory of Parallel Robot and Mechatronic System, Yanshan University, Qinhuangdao 066004, China, [2]Key Laboratory of Advanced Forging and Stamping Technology and Science, Yanshan University, Ministry of Education of China, Qinhuangdao 066004, China, [3]Academy for Engineering and Technology, Fudan University, Shanghai 200433, China, [4]College of Vehicles and Energy, Yanshan University, Qinhuangdao, Hebei 066004, China

Abstract Since the classical kinematics model of parallel manipulators cannot accurately reflect the angular velocity and angular acceleration of the limbs, an improved kinematics model is proposed and an inverse dynamic model of the general parallel manipulator is derived based on the improved kinematics model. This paper proves that the shortcoming of the classical kinematics model is that a single model cannot accurately describe the movement of several types of branches in a parallel manipulator. Combined with the principle of angular velocity superposition and vector chain method, the improved kinematic models of the general parallel manipulator's several typical limbs are derived. Then, an explicit inverse dynamic model of a general parallel robot is established based on the principle of virtual work. Finally, to describe the effectiveness of the improved model, we analyzed a new type of UP+SPR+SPU parallel manipulator. The improved models had higher accuracy than the classical models through the comparison.

1. Introduction

Compared with the serial manipulators, the multi-closed-loop structure of parallel manipulators (PMs) has a series of advantages, such as significant structural rigidity, strong carrying capacity, small error, high precision, and good dynamic performance [1, 2] and widely used in vehicle simulators [3], C.N.C. machining centers [4], high-speed picking and sorting [5], high-precision platforms [6]. To make the PMs achieve better results in engineering practice, scholars have carried out more in-depth research on type synthesis [7], kinematics [8], workspace [9], singularity [10], and dynamics [11, 12]. Among this dynamics research is the theoretical basis of dynamic performance evaluation [13], servo motor selection [14, 15], dynamic parameter identification and control [16]. Therefore, the PMs' kinematics and dynamics research is significant, but because of the P.M.s' closed-loop multi-rigid structure, its kinematics and dynamics analysis is very complicated.

At present, the dynamics, several approaches, including the Newton-Euler method, the Lagrange method, the principle of virtual work [14, 15, 17-19], have been commonly applied. Fichter et al. [20] ignored the inertia of limbs and analyzed the Gough-Stewart platform's dynamics. Tsai [21] and Wang et al. [18] introduced the virtual work principle to establish the PM's inverse dynamics model, and the form is relatively simple. Li et al. [22] used the virtual work principle to develop the inverse dynamic model of the 3-DoF (degree of freedom) module of the famous Tricept robot and the new hybrid robot TriVariant compared the dynamic characteristics of the two robots based on the inverse dynamic model. Wang et al. [13] studied the influence of placement directly on the dynamic performance of the 2-UPU+SP PM and compared the dynamic performance of the 2-UPU+SP PM with the traditional Tricept manipulator, where (P, R, U, S) represents the (prismatic, revolute, universal, spherical) joint. Rong et al. [14, 15] established the dynamic model of the 2-UPS+UPU PM configuration of the wheel grinding manipulator using the Lagrange method and estimated its driving parameters. Briot et al. [23] studied the degradation conditions of the dynamic model of the parallel manipulator and analyzed the five-bar linkage as an example.

In the literature cited above [14, 15, 17-22], to obtain the limb's angular velocity expression after deriving the vector chain, it is believed that the limb is connected to the fixed platform by U joint or S joint. The limb's angular velocity is always perpendicular to the limb's axis, and the kinematics and dynamics models are established on this basis. (This article regards the kinematics models based on the assumption that the limb's angular velocity is always perpendicular to the limb's axis as a classic model.)

However, some scholars have gradually pointed out that although this classic model simplifies the derivation process and improves the calculation efficiency, it does not conform to reality and will reduce the model's accuracy. Li et al. [24] proposed an inverse dynamics model considering the rotation of the limbs and analyzed the influence of ignoring the rotation of the outriggers around its rotation axis on the inverse kinematics solution through an example. He et al. [25] considered the rotation degree of freedom of the support rod around its axis. They improved Stewart platform's original classical dynamics model based on the Newton-Euler method. To accurately solve the manipulator's kinematics and dynamics model, Pedrammehr et al. [26] introduced the universal joint's kinematics model, considered the degree of freedom of the axial limb, and established the kinematics and dynamics of the manipulator. Lu et al. [27] used a diagonal symmetric matrix to construct the parallel manipulator motion rod's general acceleration model and Hessian matrix. Yu et al. [28] proposed a new Stewart mechanism 6-RRRPRR and established the angular velocity model of limb by numerical method.

Although previous studies tried to use different methods to establish improved models [24-28], they have mostly focused on the UPS-type limb, ignoring other types of limbs, for example, the limb linked to the base platform as a spherical joint. Therefore, it is necessary to discuss the kinematics of more types of limbs.

Based on the above reasons, we deduced the improved limb angular velocity and angular acceleration model according to the actual situation for the three main types of limbs. Taking the UP+SPR+SPU PM as the research object, the improved model was compared with the classic model, and the quality and advantages of the improved model were verified simultaneously. The research in this article aimed to make up for the shortcomings of the classical model and lay a foundation for more complex parallel manipulators' theoretical modeling.

2. Analysis of the classical kinematics model

2.1 General parallel manipulators description

In this paper, we only consider the parallel manipulators consisting of a moving platform (*m*), a base platform (*B*), and *n* limbs l_i (*i* = 1, …, *n* $\leq$ 6) (Fig. 1) for connecting *m* and *B*, each of l_i is connected with *m* at point b_i with *B* at point a_i. Let {*B*} be a coordinate frame {*o-xyz*} attached on *B* at its center *o*, {*m*} be a coordinate frame {*o′-x′y′z′*} attached on m at its center *o′*, e_i be the vector from *o′* to b_i, ${}^B_mR$ be a transform matrix from {*m*} to {*B*}. Let $\boldsymbol{v}$, $\boldsymbol{a}$ be velocity and acceleration vectors of the point *o′*. Let $\boldsymbol{\omega}$, $\boldsymbol{\varepsilon}$ be angular velocity and angular acceleration of acceleration vectors of {*m*} relative to {*B*}.

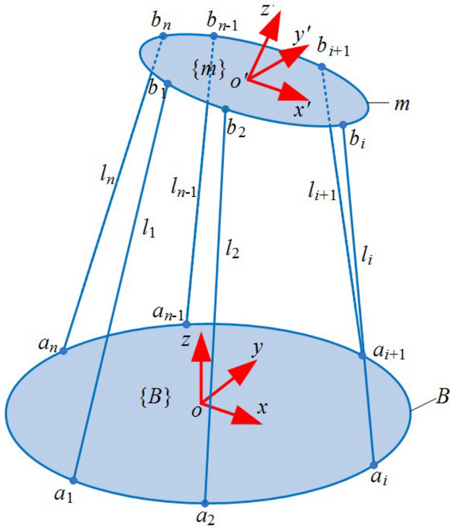

Fig. 1. A general PM with *n* limbs.

2.2 Kinematics model of limb based on principle of angular velocity superposition

As shown in Figs. 2(a) and (b), the limbs l_i of PM are connected to the base platform (*B*) through a revolute joint R_{i1}. Let $\perp$ be a perpendicular constraint, || be a parallel constraint, and | be a collinear constraint, in Fig. 2(a), the geometrical constraints $l\perp R_{i1}$, $R_{i1}\|y$ are satisfied. In Fig. 2(b), the geometrical constraints $l\perp R_{i1}$, $R_{i1}\perp y$ are satisfied. The angular velocity of the limb is derived as follows:

$$ {}^R\boldsymbol{\omega}_i = \dot{\theta}_{i1}\boldsymbol{R}_{i1} \tag{1} $$

where ${}^R\boldsymbol{\omega}_i$ is the angular velocity of the limb when the connecting joint is an R joint, $\dot{\theta}_{i1}$ is the rotational angular velocity of R_{i1}, and $\boldsymbol{R}_{i1}$ is the unit vector of the direction vector of R_{i1}. The coordinate axis of ${}^R\boldsymbol{\omega}_i$ is the axis of R_{i1} joint, and the unit vector of its axis is ${}^R\boldsymbol{w}_i$, ${}^R\boldsymbol{w}_i$ = $\boldsymbol{R}_{i1}$.Differentiating both sides of Eq. (1) concerning time leads to

$$ {}^R\boldsymbol{\varepsilon}_i = \ddot{\theta}_{i1}\boldsymbol{R}_{i1}, \dot{\boldsymbol{R}}_{i1} = 0 \tag{2} $$

where, ${}^R\boldsymbol{\varepsilon}_i$ is the limb's angular acceleration velocity when the connecting joint is an R joint.

As shown in Figs. 3(a) and (b), the PM's limbs are connected

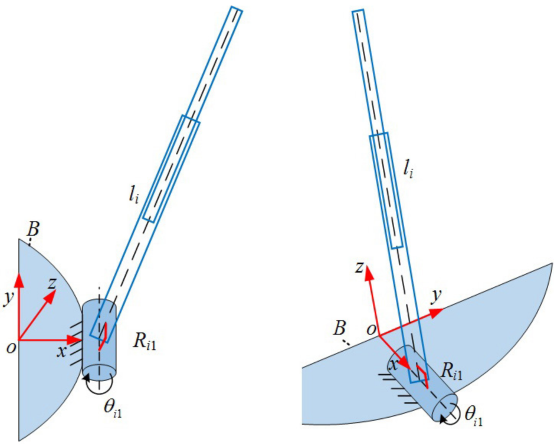

(a) (b)

Fig. 2. Installation diagram of the revolute joint: (a) $R_{i1}||y$; (b) $R_{i1}\perp y$.

to the B through U joint. U joint includes two intercrossed R joints, R_{i1} and R_{i2}. R_{i1} and R_{i2} are fixed on B and limb l_i, respectively. In Fig. 2(a), $l_i \perp R_{i2}$, $R_{i2} \perp R_{i1}$, $R_{i1}||y$ are satisfied, in Fig. 2(b), $l_i \perp R_{i2}$, $R_{i2} \perp R_{i1}$, $R_{i1} \perp y$ are satisfied. The angular velocity of the limb can be expressed as:

$$ {}^{U}\boldsymbol{\omega}_i = \dot{\theta}_{i1}\boldsymbol{R}_{i1} + \dot{\theta}_{i2}\boldsymbol{R}_{i2},\ {}^{i}\boldsymbol{R}_{i2} = \frac{\boldsymbol{R}_{i1}\times\boldsymbol{w}_i}{\left\|\boldsymbol{R}_{i1}\times\boldsymbol{w}_i\right\|} \tag{3} $$

where ${}^U\boldsymbol{\omega}_i$ is the angular velocity of the limb when the connecting joint is a U joint, $\boldsymbol{w}_i$ is the unit vector of the limb l_i, $\dot{\theta}_{ij}$ is the rotational angular velocity of R_{ij}, and $\boldsymbol{R}_{ij}$ is the unit vector the direction vector of R_{ij}. The coordinate axis of ${}^U\boldsymbol{\omega}_i$ is obtained by the combination of the R_{i1}, R_{i2} joint, and the unit vector of the coordinate axis is ${}^U\boldsymbol{w}_i$, ${}^U\boldsymbol{w}_i = \boldsymbol{R}_{i1}+\boldsymbol{R}_{i2}$. Differentiating both sides of Eq. (3) concerning time leads to

$$ {}^{U}\boldsymbol{\varepsilon}_i = \ddot{\theta}_{i1}\boldsymbol{R}_{i1} + \ddot{\theta}_{i2}\boldsymbol{R}_{i2} + \dot{\theta}_{i2}\dot{\boldsymbol{R}}_{i2},\ \dot{\boldsymbol{R}}_{i1} = 0 \tag{4} $$

where ${}^U\boldsymbol{\varepsilon}_i$ is the angular acceleration velocity of the limb when the connecting joint is a U joint, $\dot{\boldsymbol{R}}_{i2} = {}^U\boldsymbol{\omega}_i \times \boldsymbol{R}_{i2} = \dot{\theta}_{i1}\boldsymbol{R}_{i1}\times\boldsymbol{R}_{i2}$, the angular acceleration velocity ${}^U\boldsymbol{\varepsilon}_i$ as follows:

$$ {}^{U}\boldsymbol{\varepsilon}_i = \begin{bmatrix}\ddot{\theta}_{i1} & \ddot{\theta}_{i2}\end{bmatrix}\begin{bmatrix}\boldsymbol{R}_{i1}\\ \boldsymbol{R}_{i2}\end{bmatrix} + \begin{bmatrix}\dot{\theta}_{i1} & \dot{\theta}_{i2}\end{bmatrix}\begin{bmatrix}\boldsymbol{0}_{1\times 3}\\ \dot{\theta}_{i1}\boldsymbol{R}_{i1}\times\boldsymbol{R}_{i2}\end{bmatrix}. \tag{5} $$

Considering that the S joint can be equivalent to three R joints, let R_{i1} be connected to B, R_{i3} connected to the limb, R_{i1} and R_{i3} connected through R_{i2}, $R_{i1} \perp R_{i2}$, $R_{i2} \perp R_{i3}$, $R_{i3}|l_i$, the angular velocity of the limb can be expressed as follows:

$$ {}^{S}\boldsymbol{\omega}_i = \dot{\theta}_{i1}\boldsymbol{R}_{i1} + \dot{\theta}_{i2}\boldsymbol{R}_{i2} + \dot{\theta}_{i3}\boldsymbol{R}_{i3},\ \boldsymbol{R}_{i3} = \boldsymbol{w}_i \tag{6} $$

where ${}^S\boldsymbol{\omega}_i$ is the angular velocity of the limb when the connecting joint is an S joint, the coordinate axis of ${}^S\boldsymbol{\omega}_i$ is obtained by the combination of the R_{i1}, R_{i2} and R_{i3} joint, and the unit vector of the coordinate axis is ${}^S\boldsymbol{w}_i$, ${}^S\boldsymbol{w}_i = \boldsymbol{R}_{i1}+\boldsymbol{R}_{i2}+\boldsymbol{R}_{i3}$.

According to $\dot{\boldsymbol{w}}_i = \left(\dot{\theta}_{i1}\boldsymbol{R}_{i1} + \dot{\theta}_{i2}\boldsymbol{R}_{i2}\right)\times\boldsymbol{R}_{i3}$, the angular acceleration velocity ${}^S\boldsymbol{\varepsilon}_i$ is as follows:

$$ \begin{aligned} {}^{S}\boldsymbol{\varepsilon}_i = &\begin{bmatrix}\ddot{\theta}_{i1} & \ddot{\theta}_{i2} & \ddot{\theta}_{i3}\end{bmatrix}\begin{bmatrix}\boldsymbol{R}_{i1}\\ \boldsymbol{R}_{i2}\\ \boldsymbol{R}_{i3}\end{bmatrix} + \\ &\begin{bmatrix}\dot{\theta}_{i1} & \dot{\theta}_{i2} & \dot{\theta}_{i3}\end{bmatrix}\begin{bmatrix}\boldsymbol{0}_{1\times 3}\\ \dot{\theta}_{i1}\boldsymbol{R}_{i1}\times\boldsymbol{R}_{i2}\\ \left(\dot{\theta}_{i1}\boldsymbol{R}_{i1}+\dot{\theta}_{i2}\boldsymbol{R}_{i2}\right)\times\boldsymbol{R}_{i3}\end{bmatrix}. \end{aligned} \tag{7} $$

2.3 Limitations of the classical kinematics model of the limb

Suppose $\boldsymbol{\rho} = [\rho_x \rho_y \rho_z]^{\mathrm{T}}$, $\boldsymbol{\chi} = [\chi_x \chi_y \chi_z]^{\mathrm{T}}$ are two arbitrary vectors and a skew-symmetric matrix

$$ \hat{\boldsymbol{\rho}} = \begin{bmatrix} 0 & -\rho_z & \rho_y \\ \rho_z & 0 & -\rho_x \\ -\rho_y & \rho_x & 0 \end{bmatrix}, \boldsymbol{\rho}\times\boldsymbol{\chi} = \hat{\boldsymbol{\rho}}\boldsymbol{\chi}. \tag{8} $$

In the general PM shown in Fig. 1, the velocity of point b_i can be expressed as

$$ \boldsymbol{v}_i = \dot{l}_i\boldsymbol{w}_i + l_i\boldsymbol{\omega}_i\times\boldsymbol{w}_i. \tag{9} $$

Cross-multiplying both sides of Eq. (9) by $\boldsymbol{w}_i$ leads to

$$ \boldsymbol{w}_i\times\boldsymbol{v}_i = l_i\left(\boldsymbol{\omega}_i - \left(\boldsymbol{\omega}_i^T\boldsymbol{w}_i\right)\boldsymbol{w}_i\right). \tag{10} $$

The classical model considered that U or S joint could not rotate about its longitudinal axis such that $\boldsymbol{\omega}_i^T\boldsymbol{w}_i = 0$. Let $\boldsymbol{v}$ be the translational velocity of point o', $\boldsymbol{\omega}$ be angular velocity of {m} relative to {B}, the angular velocity of the limb can be expressed as

$$ {}^{*}\boldsymbol{\omega}_i = \frac{\hat{\boldsymbol{w}}_i\boldsymbol{v}_i}{l_i} = \frac{\hat{\boldsymbol{w}}_i}{l_i}\left[\boldsymbol{E}_3 \ \ -\hat{\boldsymbol{e}}_i\right]\begin{bmatrix}\boldsymbol{v}\\ \boldsymbol{\omega}\end{bmatrix} = {}^{*}\boldsymbol{J}_{\omega i}\boldsymbol{V}, \boldsymbol{E}_3 = \begin{bmatrix}1\,0\,0\\ 0\,1\,0\\ 0\,0\,1\end{bmatrix} \tag{11} $$

where ${}^*\boldsymbol{\omega}_i$ is the angular velocity of the classical model; differentiating both sides of Eq. (11) to time leads to

$$ \begin{aligned} &{}^{*}\boldsymbol{\varepsilon}_i = {}^{*}\dot{\boldsymbol{J}}_{\omega i}\boldsymbol{V} + {}^{*}\boldsymbol{J}_{\omega i}\dot{\boldsymbol{V}} \\ &{}^{*}\dot{\boldsymbol{J}}_{\omega i} = -\frac{\dot{l}_i}{l_i^2}\left[\hat{\boldsymbol{w}}_i \ \ -\hat{\boldsymbol{w}}_i\hat{\boldsymbol{e}}_i\right] + \\ &\qquad \frac{1}{l_i}\left[\widehat{\left(\boldsymbol{\omega}_i\times\boldsymbol{w}_i\right)} \ \ -\widehat{\left(\boldsymbol{\omega}_i\times\boldsymbol{w}_i\right)}\hat{\boldsymbol{e}}_i - \hat{\boldsymbol{w}}_i\widehat{\left(\boldsymbol{\omega}\times\boldsymbol{e}_i\right)}\right] \\ &\dot{l}_i = \boldsymbol{J}_{mi}\boldsymbol{V}, \boldsymbol{J}_{mi} = \left[\boldsymbol{w}_i^{\mathrm{T}} \ \ \left(\boldsymbol{e}_i\times\boldsymbol{w}_i\right)^{\mathrm{T}}\right]. \end{aligned} \tag{12} $$

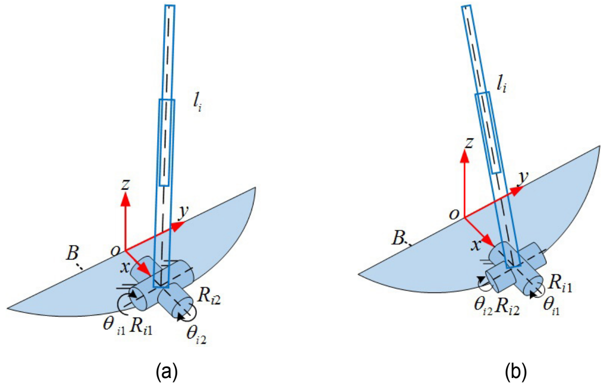

Fig. 3. Installation diagram of the universal joint: (a) $R_{i1}||y$; (b) $R_{i1}\perp y$.

Eqs. (11) and (12) together constitute the classical kinematics model. According to Eqs. (10)-(12), the prerequisite for the establishment of the classical model is that $\boldsymbol{\omega}_i^T \boldsymbol{w}_i$ = 0. It can be seen from Fig. 3 that the U joint consists of R_{i1} and R_{i2}, $R_{i2}\perp l_i$, $R_{i2}\cdot w_i$ = 0, so there will be

$$^{U}\boldsymbol{\omega}_i\cdot\boldsymbol{w}_i=\left(\dot{\theta}_{i1}\boldsymbol{R}_{i1}+\dot{\theta}_{i2}\boldsymbol{R}_{i2}\right)\cdot\boldsymbol{w}_i=\dot{\theta}_{i1}\boldsymbol{R}_{i1}\cdot\boldsymbol{w}_i\ . \tag{13}$$

According to Eq. (13), $^{U}\boldsymbol{\omega}_i^T\boldsymbol{w}_i\neq 0$, so the classical model cannot be applied to the limb in Fig. 3. Similarly, from Eq. (6), there will be $^{S}\boldsymbol{\omega}_i\cdot\boldsymbol{w}_i=\dot{\theta}_{i1}\boldsymbol{R}_{i1}\cdot\boldsymbol{w}_i+\dot{\theta}_{i3}\boldsymbol{R}_{i3}\cdot\boldsymbol{w}_i$, the limb connected to the based platform through S joint, the kinematics of the limb cannot be represented by the classical model. In addition, the Refs. [24-27] also discusses the limitations of the classic model from other perspectives, which will not be described in this article.

3. Analysis of the improved kinematics model

Although the angular velocity and angular acceleration models of different types of joints are derived based on the principle of angular velocity superposition in Sec. 2.2, the rotational angular velocity is difficult to obtain directly, so this section will further derive the formula in Sec. 2.3.

3.1 Improved kinematics model of $^R\omega$ and $^R\varepsilon$

According to the above description in Sec. 2 , there can be

$$^{R}\omega_i={}^{*}\omega_i,\ {}^{R}\varepsilon_i={}^{*}\varepsilon_i\ . \tag{14}$$

3.2 Improved kinematics model of $^U\omega$ and $^U\varepsilon$

Cross multiplying both sides of Eq. (3) by R_{i1}, R_{i2} leads to

$$\boldsymbol{R}_{i1}\times{}^{U}\boldsymbol{\omega}_i=\dot{\theta}_{i2}\left(\boldsymbol{R}_{i1}\times\boldsymbol{R}_{i2}\right) \tag{15}$$

$$\boldsymbol{R}_{i2}\times{}^{U}\boldsymbol{\omega}_i=\dot{\theta}_{i1}\left(\boldsymbol{R}_{i2}\times\boldsymbol{R}_{i1}\right)\ . \tag{16}$$

Dot multiplying both sides of Eq. (9) by R_{i1} and R_{i2}, respectively, leads to

$$\begin{aligned}&\boldsymbol{R}_{i1}^{\mathrm{T}}\boldsymbol{v}_i=\boldsymbol{R}_{i1}\cdot\dot{l}_i\boldsymbol{w}_i+l_i\boldsymbol{R}_{i1}\cdot\left({}^{U}\boldsymbol{\omega}_i\times\boldsymbol{w}_i\right)=\\&\boldsymbol{R}_{i1}^{\mathrm{T}}\boldsymbol{w}_i\boldsymbol{w}_i^{\mathrm{T}}\left(\boldsymbol{v}-\hat{\boldsymbol{e}}_i\boldsymbol{\omega}\right)+l_i\boldsymbol{w}_i\cdot\left(\boldsymbol{R}_{i1}\times{}^{U}\boldsymbol{\omega}_i\right)\end{aligned} \tag{17}$$

$$\begin{aligned}&\boldsymbol{R}_{i2}^{\mathrm{T}}\boldsymbol{v}_i=\boldsymbol{R}_{i2}\cdot\boldsymbol{w}_i\left(\boldsymbol{w}_i\cdot\boldsymbol{v}_i\right)+l_i\boldsymbol{R}_{i2}\cdot\left({}^{U}\boldsymbol{\omega}_i\times\boldsymbol{w}_i\right)=\\&\boldsymbol{R}_{i2}^{\mathrm{T}}\boldsymbol{w}_i\boldsymbol{w}_i^{\mathrm{T}}\left(\boldsymbol{v}-\hat{\boldsymbol{e}}_i\boldsymbol{\omega}\right)+l_i\boldsymbol{w}_i\cdot\left(\boldsymbol{R}_{i2}\times{}^{U}\boldsymbol{\omega}_i\right).\end{aligned} \tag{18}$$

Substituting Eqs. (13) and (14) into Eqs. (15) and (16), respectively, leads to

$$\dot{\theta}_{i1}=\frac{\left(\boldsymbol{R}_{i2}^{\mathrm{T}}\hat{\boldsymbol{w}}_i^2\right)\left(\boldsymbol{v}-\hat{\boldsymbol{e}}_i\boldsymbol{\omega}\right)}{l_i\boldsymbol{w}_i\cdot\left(\left(\boldsymbol{R}_{i1}\times\boldsymbol{R}_{i2}\right)\right)},\dot{\theta}_{i2}=\frac{-\left(\boldsymbol{R}_{i1}^{\mathrm{T}}\hat{\boldsymbol{w}}_i^2\right)\left(\boldsymbol{v}-\hat{\boldsymbol{e}}_i\boldsymbol{\omega}\right)}{l_i\boldsymbol{w}_i\cdot\left(\left(\boldsymbol{R}_{i1}\times\boldsymbol{R}_{i2}\right)\right)}\ . \tag{19}$$

Substituting Eq. (19) into Eq. (3), $^{U}\boldsymbol{\omega}_i$ is derived as follows:

$$\begin{aligned}&^{U}\boldsymbol{\omega}_i=\dot{\theta}_{i1}\boldsymbol{R}_{i1}+\dot{\theta}_{i2}\boldsymbol{R}_{i2}={}^{U}\boldsymbol{J}_{\omega i}\boldsymbol{V}\\&^{U}\boldsymbol{J}_{\omega i}=\left[\frac{\left(\boldsymbol{R}_{i1}\boldsymbol{R}_{i2}^{\mathrm{T}}-\boldsymbol{R}_{i2}\boldsymbol{R}_{i1}^{\mathrm{T}}\right)\hat{\boldsymbol{w}}_i^2}{\left(\boldsymbol{R}_{i1}\times\boldsymbol{R}_{i2}\right)\cdot l_i\boldsymbol{w}_i}\quad-\frac{\left(\boldsymbol{R}_{i1}\boldsymbol{R}_{i2}^{\mathrm{T}}-\boldsymbol{R}_{i2}\boldsymbol{R}_{i1}^{\mathrm{T}}\right)\hat{\boldsymbol{w}}_i^2\hat{\boldsymbol{e}}_i}{\left(\boldsymbol{R}_{i1}\times\boldsymbol{R}_{i2}\right)\cdot l_i\boldsymbol{w}_i}\right].\end{aligned} \tag{20}$$

Differentiating both sides of Eq. (20) to time leads to

$$^{U}\boldsymbol{\varepsilon}_i={}^{U}\dot{\boldsymbol{J}}_{\omega i}\boldsymbol{V}+{}^{U}\boldsymbol{J}_{\omega i}\dot{\boldsymbol{V}}\ . \tag{21}$$

Eqs. (20) and (21) are the improved $^{U}\boldsymbol{\omega}_i$ and $^{U}\boldsymbol{\varepsilon}_i$ models of a limb when the point b_i is a U joint. Eq. (6) represents the situation where the third R joint of the three R joints equivalent to the S joint at point ai is collinear with the limb, and a more detailed analysis is needed to obtain a general model.

3.3 Improved kinematics model of SPR-type or SR-type limb

If point a_i in Fig. 1 is the S joint, and point b_i is an R joint, then the angular velocity of SPR-type or SR-type limb can be represented as:

$$^{SPR\&SR}\boldsymbol{\omega}_i=\boldsymbol{\omega}-\dot{\theta}_{i1}\boldsymbol{R}_{i1}\ . \tag{22}$$

Dot multiplying both sides of Eq. (22) by $\boldsymbol{w}_i$ leads to below

$$\begin{aligned}&^{SPR\&SR}\boldsymbol{\omega}_i={}^{SPR\&SR}\boldsymbol{J}_{\omega i}\boldsymbol{V}\\&^{SPR\&SR}\boldsymbol{J}_{\omega i}=\frac{1}{l_i}\left[\hat{\boldsymbol{w}}_i\quad-\hat{\boldsymbol{w}}_i\hat{\boldsymbol{e}}_i+l_i\boldsymbol{w}_i\boldsymbol{w}_i^{\mathrm{T}}\right].\end{aligned} \tag{23}$$

Differentiating both sides of Eq. (23) for time leads to

$$^{SPR\&SR}\boldsymbol{\varepsilon}_i={}^{SPR\&SR}\dot{\boldsymbol{J}}_{\omega i}\boldsymbol{V}+{}^{SPR\&SR}\boldsymbol{J}_{\omega i}\dot{\boldsymbol{V}} \tag{24}$$

where $^{SPR\&SP}\varepsilon_i$ is the angular acceleration velocity of SPR-type or SR-type limb.

3.4 Improved kinematics model of SPU-type or SU-type limb

If point a_i in Fig. 1 is the S joint, and point b_i is the U joint, the U joint at b_i includes two intercrossed R joints R_{i1} and R_{i2}, R_{i1} and R_{i2} base m and limb l_i, respectively. Then, the angular velocity of SPU-type or SU-type limb can be represented as:

$$ {}^{SPU\&SU}\boldsymbol{\omega}_i = \boldsymbol{\omega} - \dot{\theta}_{i1}\boldsymbol{R}_{i1} - \dot{\theta}_{i2}\boldsymbol{R}_{i2} . \tag{25} $$

Cross multiplying both sides of Eq. (25) by R_{i1}, R_{i2} leads to

$$ \boldsymbol{R}_{i1} \times {}^{SPU\&SU}\boldsymbol{\omega}_i = \boldsymbol{R}_{i1} \times \boldsymbol{\omega} - \dot{\theta}_{i2}\boldsymbol{R}_{i1} \times \boldsymbol{R}_{i2} \tag{26} $$

$$ \boldsymbol{R}_{i2} \times {}^{SPU\&SU}\boldsymbol{\omega}_i = \boldsymbol{R}_{i2} \times \boldsymbol{\omega} - \dot{\theta}_{i1}\boldsymbol{R}_{i2} \times \boldsymbol{R}_{i1} . \tag{27} $$

Dot multiplying both sides of Eq. (9) by R_{i1} and R_{i2}, respectively, leads to

$$ \begin{aligned} &\boldsymbol{R}_{i1}^{\mathrm{T}}\boldsymbol{v}_i = \boldsymbol{R}_{i1} \cdot \dot{l}_i\boldsymbol{w}_i + l_i\boldsymbol{R}_{i1} \cdot \left({}^{SPU\&SU}\boldsymbol{\omega}_i \times \boldsymbol{w}_i \right) = \\ &\boldsymbol{R}_{i1}^{\mathrm{T}}\boldsymbol{w}_i\boldsymbol{w}_i^{\mathrm{T}}\left(\boldsymbol{v} - \hat{\boldsymbol{e}}_i\boldsymbol{\omega}\right) + l_i\boldsymbol{w}_i \cdot \left(\boldsymbol{R}_{i1} \times \boldsymbol{\omega} - \dot{\theta}_{i2}\boldsymbol{R}_{i1} \times \boldsymbol{R}_{i2}\right) \end{aligned} \tag{28} $$

$$ \begin{aligned} &\boldsymbol{R}_{i2}^{\mathrm{T}}\boldsymbol{v}_i = \boldsymbol{R}_{i2} \cdot \dot{l}_i\boldsymbol{w}_i + l_i\boldsymbol{R}_{i2} \cdot \left({}^{SPU\&SU}\boldsymbol{\omega}_i \times \boldsymbol{w}_i \right) = \\ &\boldsymbol{R}_{i2}^{\mathrm{T}}\boldsymbol{w}_i\boldsymbol{w}_i^{\mathrm{T}}\left(\boldsymbol{v} - \hat{\boldsymbol{e}}_i\boldsymbol{\omega}\right) + l_i\boldsymbol{w}_i \cdot \left(\boldsymbol{R}_{i2} \times \boldsymbol{\omega} - \dot{\theta}_{i1}\boldsymbol{R}_{i2} \times \boldsymbol{R}_{i1}\right). \end{aligned} \tag{29} $$

Substituting Eqs. (28) and (29) into Eqs. (26) and (27), respectively, it leads to

$$ \begin{aligned} \dot{\theta}_{i1} &= \frac{\boldsymbol{R}_{i2} \cdot \left(l_i\hat{\boldsymbol{w}}_i\boldsymbol{\omega}\right) - \left(\hat{\boldsymbol{w}}_i^2\boldsymbol{v} - \hat{\boldsymbol{w}}_i^2\hat{\boldsymbol{e}}_i\boldsymbol{\omega}\right) \cdot \boldsymbol{R}_{i2}}{\left(\boldsymbol{R}_{i1} \times \boldsymbol{R}_{i2}\right) \cdot l_i\boldsymbol{w}_i} \\ \dot{\theta}_{i2} &= \frac{-\boldsymbol{R}_{i1} \cdot \left(l_i\hat{\boldsymbol{w}}_i\boldsymbol{\omega}\right) + \left(\hat{\boldsymbol{w}}_i^2\boldsymbol{v} - \hat{\boldsymbol{w}}_i^2\hat{\boldsymbol{e}}_i\boldsymbol{\omega}\right) \cdot \boldsymbol{R}_{i1}}{\left(\boldsymbol{R}_{i1} \times \boldsymbol{R}_{i2}\right) \cdot l_i\boldsymbol{w}_i}. \end{aligned} \tag{30} $$

From Eq. (30), the combined rotational angular velocity of R_{i2} and R_{i1}, ${}^{SPU\&SU}\boldsymbol{\omega}_i$ is derived as follows:

$$ \begin{aligned} &{}^{SPU\&SU}\boldsymbol{\omega}_i = \boldsymbol{\omega} - \dot{\theta}_{i1}\boldsymbol{R}_{i1} - \dot{\theta}_{i2}\boldsymbol{R}_{i2} = {}^{SPU\&SU}\boldsymbol{J}_{\omega i}\boldsymbol{V} \\ &{}^{SPU\&SU}\boldsymbol{J}_{\omega i} = \begin{bmatrix} \dfrac{\left(\boldsymbol{R}_{i1}\boldsymbol{R}_{i2}^{\mathrm{T}} - \boldsymbol{R}_{i2}\boldsymbol{R}_{i1}^{\mathrm{T}}\right)\hat{\boldsymbol{w}}_i^2}{\left(\boldsymbol{R}_{i1} \times \boldsymbol{R}_{i2}\right) \cdot l_i\boldsymbol{w}_i} \\ \dfrac{-\left(\boldsymbol{R}_{i1}\boldsymbol{R}_{i2}^{\mathrm{T}} - \boldsymbol{R}_{i2}\boldsymbol{R}_{i1}^{\mathrm{T}}\right)\left(l_i\hat{\boldsymbol{w}}_i + \hat{\boldsymbol{w}}_i^2\hat{\boldsymbol{e}}_i\right)}{\left(\boldsymbol{R}_{i1} \times \boldsymbol{R}_{i2}\right) \cdot l_i\boldsymbol{w}_i} + \boldsymbol{E}_{3\times3} \end{bmatrix}^{\mathrm{T}}. \end{aligned} \tag{31} $$

Differentiating both sides of Eq. (31) to time leads to

$$ {}^{SPU\&SU}\boldsymbol{\varepsilon}_i = {}^{SPU\&SU}\dot{\boldsymbol{J}}_{\omega i}\boldsymbol{V} + {}^{SPU\&SU}\boldsymbol{J}_{\omega i}\dot{\boldsymbol{V}} \tag{32} $$

where ${}^{SPU\&SU}\varepsilon_i$ is the angular acceleration velocity of SPR-type or SR-type limb.

Let $\boldsymbol{\omega}_i$, $\boldsymbol{\varepsilon}_i$, $\boldsymbol{J}_\omega$, $\dot{\boldsymbol{J}}_{\omega i}$ be the set of angular velocities, angular accelerations, matrices, and differential matrices under different types of limbs in Sec. 3, which can be represented as

$$ \begin{aligned} &\boldsymbol{\omega}_i = \boldsymbol{J}_{\omega i}\boldsymbol{V}, \boldsymbol{\varepsilon}_i = \dot{\boldsymbol{J}}_{\omega i}\boldsymbol{V} + \boldsymbol{J}_{\omega i}\dot{\boldsymbol{V}}, \\ &\boldsymbol{\omega}_i = \left\{ {}^{*}\boldsymbol{\omega}_i, {}^{R}\boldsymbol{\omega}_i, {}^{U}\boldsymbol{\omega}_i, {}^{SPR\&SR}\boldsymbol{\omega}_i, {}^{SPU\&SU}\boldsymbol{\omega}_i \right\}, \\ &\boldsymbol{\varepsilon}_i = \left\{ {}^{*}\boldsymbol{\varepsilon}_i, {}^{R}\boldsymbol{\varepsilon}_i, {}^{U}\boldsymbol{\varepsilon}_i, {}^{SPR\&SR}\boldsymbol{\varepsilon}_i, {}^{SPU\&SU}\boldsymbol{\varepsilon}_i \right\}, \\ &\boldsymbol{J}_{\omega i} = \left\{ {}^{*}\boldsymbol{J}_{\omega i}, {}^{R}\boldsymbol{J}_{\omega i}, {}^{U}\boldsymbol{J}_{\omega i}, {}^{SPR\&SR}\boldsymbol{J}_{\omega i}, {}^{SPU\&SU}\boldsymbol{J}_{\omega i} \right\}, \\ &\dot{\boldsymbol{J}}_{\omega i} = \left\{ {}^{*}\dot{\boldsymbol{J}}_{\omega i}, {}^{R}\dot{\boldsymbol{J}}_{\omega i}, {}^{U}\dot{\boldsymbol{J}}_{\omega i}, {}^{SPR\&SR}\dot{\boldsymbol{J}}_{\omega i}, {}^{SPU\&SU}\dot{\boldsymbol{J}}_{\omega i} \right\}. \end{aligned} \tag{33} $$

The improved model is more in line with the kinematics of the limb than the classical model; compared with previous studies that mostly considered UPS-type limb, this paper improves the kinematics of multiple types of limbs. Compared with the approximate solution obtained by the numerical iterative method used in the Ref. [28], the model derived in this paper is an analytical solution directly expressed by mathematical expressions.

4. Inverse dynamics model of general parallel manipulators

Aiming at the limitations of classical kinematics, the third chapter establishes an improved kinematics model. To further discuss the influence of the improved kinematics model on dynamics, a general inverse dynamics model needs to be established.

If each limb of the general PM shown in Fig. 1 is linearly driven, each limb l_i is composed of a piston rod and a cylinder. The piston rod of l_i is connected with *m* at b_i, the cylinder of l_i is connected with *B* at a_i, respectively. Let p_i be the mass center of the piston rod in l_i, l_{pi} be the distance from b_i to p_i; c_i be the mass center of the cylinder in l_i and l_{ci} be the distance from a_i to c_i.

Let $\boldsymbol{v}_{ci}$, $\boldsymbol{v}_{pi}$, $\boldsymbol{\omega}_{ci}$, $\boldsymbol{\omega}_{pi}$, $\boldsymbol{a}_{ci}$, $\boldsymbol{a}_{pi}$, $\boldsymbol{\varepsilon}_{ci}$, $\boldsymbol{\varepsilon}_{pi}$ be the translational velocity, angular velocity, the translational acceleration, the angular acceleration. The translational velocity $\boldsymbol{v}_{ci}$ and $\boldsymbol{v}_{pi}$ in {B} are expressed as follows:

$$ \begin{aligned} &\boldsymbol{v}_{ci} = \boldsymbol{J}_{ci}\boldsymbol{V}, \ \boldsymbol{\omega}_{ci} = \boldsymbol{\omega}_i, \ \boldsymbol{J}_{ci} = -l_{ci}\hat{\boldsymbol{w}}_i\boldsymbol{J}_{\omega i}, \\ &\boldsymbol{v}_{pi} = \boldsymbol{J}_{pi}\boldsymbol{V}, \ \boldsymbol{J}_{pi} = -\left(l_i - l_{pi}\right)\hat{\boldsymbol{w}}_i\boldsymbol{J}_{\omega i} + \boldsymbol{w}_i\boldsymbol{J}_{mi}, \\ &\boldsymbol{V}_{ci} = \begin{bmatrix} \boldsymbol{v}_{ci} \\ \boldsymbol{\omega}_i \end{bmatrix} = \boldsymbol{J}_{ci}\boldsymbol{V}, \boldsymbol{J}_{Ci} = \begin{bmatrix} \boldsymbol{J}_{ci} \\ \boldsymbol{J}_{\omega i} \end{bmatrix} \\ &\boldsymbol{V}_{pi} = \begin{bmatrix} \boldsymbol{v}_{pi} \\ \boldsymbol{\omega}_i \end{bmatrix} = \boldsymbol{J}_{Pi}\boldsymbol{V}, \boldsymbol{J}_{Pi} = \begin{bmatrix} \boldsymbol{J}_{pi} \\ \boldsymbol{J}_{\omega i} \end{bmatrix} \end{aligned} \tag{34} $$

where $\boldsymbol{\omega}_i$, and $\boldsymbol{J}_{\omega i}$, in Eq. (34) are the set defined in the previous section. If the type of joint in the limb X.P.X. is determined, the corresponding subset in the set can be determined to achieve the role of a universal model; differentiating Eq. (34) to time leads to

$$ \begin{aligned} &\boldsymbol{a}_{ci} = \dot{\boldsymbol{J}}_{ci}\boldsymbol{V} + \boldsymbol{J}_{ci}\dot{\boldsymbol{V}}, \ \dot{\boldsymbol{J}}_{ci} = -l_{ci}\left(\dot{\hat{\boldsymbol{w}}}_i\boldsymbol{J}_{\omega i} + \hat{\boldsymbol{w}}_i\dot{\boldsymbol{J}}_{\omega i}\right) \\ &\boldsymbol{a}_{pi} = \dot{\boldsymbol{J}}_{pi}\boldsymbol{V}_o + \boldsymbol{J}_{pi}\dot{\boldsymbol{V}}_o \end{aligned} $$

$$\dot{\boldsymbol{J}}_{pi}=\begin{pmatrix}-(\boldsymbol{J}_{mi}V)\hat{\boldsymbol{w}}_i\boldsymbol{J}_{\omega i}-(l_i-l_{pi})\widehat{(\boldsymbol{\omega}_i\times\boldsymbol{w}_i)}\boldsymbol{J}_{\omega i}-\\(l_i-l_{pi})\hat{\boldsymbol{w}}_i\dot{\boldsymbol{J}}_{\omega i}+(\boldsymbol{\omega}_i\times\boldsymbol{w}_i)\boldsymbol{J}_{mi}+\boldsymbol{w}_i\dot{\boldsymbol{J}}_{mi}\end{pmatrix}$$
$$\dot{\boldsymbol{J}}_{mi}=\left[(\boldsymbol{\omega}_i\times\boldsymbol{w}_i)^{\mathrm{T}}\quad\left((\boldsymbol{\omega}_i\times\boldsymbol{e}_i)\times\boldsymbol{w}_i+\boldsymbol{e}_i\times(\boldsymbol{\omega}_i\times\boldsymbol{w}_i)\right)^{\mathrm{T}}\right].\tag{35}$$

Let m_o, $\boldsymbol{G}_o$, $\boldsymbol{f}_o$, $\boldsymbol{n}_o$, and $\boldsymbol{I}_o$ be the mass, the gravity, inertia force, inertia torque, and the inertia matrix of the moving platform *m*. Let m_{ci}, $\boldsymbol{G}_{ci}$, $\boldsymbol{f}_{ci}$, $\boldsymbol{n}_{ci}$, and $\boldsymbol{I}_{ci}$ be the mass, the gravity, inertia force, inertia torque, and the inertia matrix of the cylinder of the limb li, respectively. Let m_{pi}, $\boldsymbol{G}_p$, $\boldsymbol{f}_{pi}$, $\boldsymbol{n}_{pi}$, and $\boldsymbol{I}_{pi}$ be the mass, gravity, inertia force, inertia torque, and the piston's inertia matrix rod of the limb l_i, respectively. Let R_{il} denote the revolute joint fixedly connected with the limb; if the connecting joint is an R joint, $R_{il}=R_{i1}$, if the connecting joint is a U or S joint, $R_{il}=R_{i2}$. Let $\boldsymbol{R}_{il}$ is the unit vector of R_{il}. The gravity, inertia force, torque, and inertia matrix can be derived as follows:

$$\begin{aligned}&\boldsymbol{G}_o=m_o\boldsymbol{g},\boldsymbol{f}_o=-m_o\boldsymbol{a},\boldsymbol{n}_o=-\tilde{\boldsymbol{I}}_o\boldsymbol{\varepsilon}-\boldsymbol{\omega}\times\left[\tilde{\boldsymbol{I}}_o\boldsymbol{\omega}\right]\\&\boldsymbol{G}_{ci}=m_{ci}\boldsymbol{g},\boldsymbol{f}_{ci}=-m_{ci}\boldsymbol{a}_{ci},\boldsymbol{n}_{ci}=-\tilde{\boldsymbol{I}}_{ci}\boldsymbol{\varepsilon}_{ci}-\boldsymbol{\omega}_{ci}\times\left[\tilde{\boldsymbol{I}}_{ci}\boldsymbol{\omega}_{ci}\right]\\&\boldsymbol{G}_{pi}=m_{pi}\boldsymbol{g},\boldsymbol{f}_{pi}=-m_{pi}\boldsymbol{a}_{pi},\boldsymbol{n}_{pi}=-\tilde{\boldsymbol{I}}_{pi}\boldsymbol{\varepsilon}_{pi}-\boldsymbol{\omega}_{pi}\times\left[\tilde{\boldsymbol{I}}_{pi}\boldsymbol{\omega}_{pi}\right]\\&\boldsymbol{R}_i=\left[\boldsymbol{R}_{il}\quad\boldsymbol{w}_i\times\boldsymbol{R}_{il}\quad\boldsymbol{w}_i\right],\tilde{\boldsymbol{I}}_o=\left({}_m^B\boldsymbol{R}\right)\boldsymbol{I}_o\left({}_m^B\boldsymbol{R}\right)^{\mathrm{T}}\\&\tilde{\boldsymbol{I}}_{ci}=(\boldsymbol{R}_i)\boldsymbol{I}_{ci}(\boldsymbol{R}_i)^{\mathrm{T}},\tilde{\boldsymbol{I}}_{pi}=(\boldsymbol{R}_i)\boldsymbol{I}_{pi}(\boldsymbol{R}_i)^{\mathrm{T}}\end{aligned}\tag{36}$$

where $\boldsymbol{R}_i$ denotes the rotational matrix of {*i*} relative to {*B*}. {*i*} is a coordinate frame with $\boldsymbol{R}_{il}$, $\boldsymbol{w}_i\times\boldsymbol{R}_{il}$, and $\boldsymbol{w}_i$ are the diction vectors corresponding to their three orthogonal coordinate axes, which are used to express the inertia matrices.

Let $\boldsymbol{F}$ and $\boldsymbol{T}$ be the force and torque applied on *m* at o'. Let $\boldsymbol{F}_q$ be the general dynamic input forces. From the principle of virtual work, it leads to

$$\boldsymbol{F}_q^{\mathrm{T}}\boldsymbol{J}_{mi}\begin{bmatrix}\boldsymbol{v}\\\boldsymbol{\omega}\end{bmatrix}+\left[\boldsymbol{F}^{\mathrm{T}}+\boldsymbol{f}_o^{\mathrm{T}}+\boldsymbol{G}_o^{\mathrm{T}}\quad\boldsymbol{T}^{\mathrm{T}}+\boldsymbol{n}_o^{\mathrm{T}}\right]\begin{bmatrix}\boldsymbol{v}\\\boldsymbol{\omega}\end{bmatrix}+\sum_{i=1}^{n(2\le n\le 6)}\begin{pmatrix}\left[\boldsymbol{f}_{ci}^{\mathrm{T}}+\boldsymbol{G}_{ci}^{\mathrm{T}}\quad\boldsymbol{n}_{ci}^{\mathrm{T}}\right]\boldsymbol{J}_{Ci}\begin{bmatrix}\boldsymbol{v}\\\boldsymbol{\omega}\end{bmatrix}+\\\left[\boldsymbol{f}_{pi}^{\mathrm{T}}+\boldsymbol{G}_{pi}^{\mathrm{T}}\quad\boldsymbol{n}_{pi}^{\mathrm{T}}\right]\boldsymbol{J}_{Pi}\begin{bmatrix}\boldsymbol{v}\\\boldsymbol{\omega}\end{bmatrix}\end{pmatrix}=0.\tag{37}$$

If 2 ≤ *n* ≤ 6, the PM is shown in Fig. 1 is a limited degrees of freedom PM, and Eq. (37) needs to introduce velocity decoupling matrix $\boldsymbol{J}_{B.}$ in the form of 6×*n*, a formula for solving the inverse dynamic input forces is derived as below:

$$\boldsymbol{F}_q=-\left(\boldsymbol{J}_D^{-1}\right)^{\mathrm{T}}\boldsymbol{J}_B^{\mathrm{T}}\begin{bmatrix}\boldsymbol{F}+\boldsymbol{f}_o+\boldsymbol{G}_o\\\boldsymbol{T}+\boldsymbol{n}_o\end{bmatrix}-\left(\boldsymbol{J}_D^{-1}\right)^{\mathrm{T}}\boldsymbol{J}_B^{\mathrm{T}}\sum_{i=1}^{n(2\le n\le 6)}\begin{pmatrix}\boldsymbol{J}_{Ci}^{\mathrm{T}}\begin{bmatrix}\boldsymbol{f}_{ci}+\boldsymbol{G}_{ci}\\\boldsymbol{n}_{ci}\end{bmatrix}+\\\boldsymbol{J}_{Pi}^{\mathrm{T}}\begin{bmatrix}\boldsymbol{f}_{pi}+\boldsymbol{G}_{pi}\\\boldsymbol{n}_{pi}\end{bmatrix}\end{pmatrix}$$
$$\boldsymbol{J}_D=\boldsymbol{J}_{im}\boldsymbol{J}_B.\tag{38}$$

Substituting Eqs. (33) and (35) into Eq. (38) leads to

$$\boldsymbol{F}_q=\boldsymbol{D}\dot{\boldsymbol{V}}+\boldsymbol{H}\boldsymbol{V}+\boldsymbol{G}+\boldsymbol{E}.\tag{39}$$

According to the description of the physical meanings of the dynamic model in the Ref. [29], $\boldsymbol{D}$ is the inertia matrix, $\boldsymbol{HV}$ involves the Coriolis and viscous damping forces. $\boldsymbol{G}$ is the driving force required to compensate for the gravity factor of the manipulator, and $\boldsymbol{E}$ is the driving force needed to compensate for the load of the MP, the complete formula of Eq. (39) is in the Appendix.

5. Example

5.1 Parallel manipulators description and position analysis

In this section, UP+SPR+SPU PM (see Fig. 4) is selected as the research object to compare the classic model and the improved model, this manipulator consists of a base platform *B*, a moving platform *m*, and a UP-type limb l_1, an SPR-type limb l_2, and an SPU-type limb l_3 so that a UP+SPR +SPU PM can verify the kinematic models of three typical limbs. The *B*, *m* of UP+SPR+ SPU PM are isosceles right-angled triangles with three vertices a_i and b_i (*i* = 1, 2, 3). UP-type limb connects *B* with *m* by a universal joint U at a_1, an active limb l_1 with prismatic joint P along it and the other end of the P joint is fixed to *m*. SPR-type limb connects *B* with *m* by a spherical joint at a_2, an active limb l_2 with prismatic joint P along it and one revolute joint at b_2. SPU-type limb connects *B* with *m* by a spherical joint at a_3, an active limb l_3 with prismatic joint P along it and one universal joint at b_3.

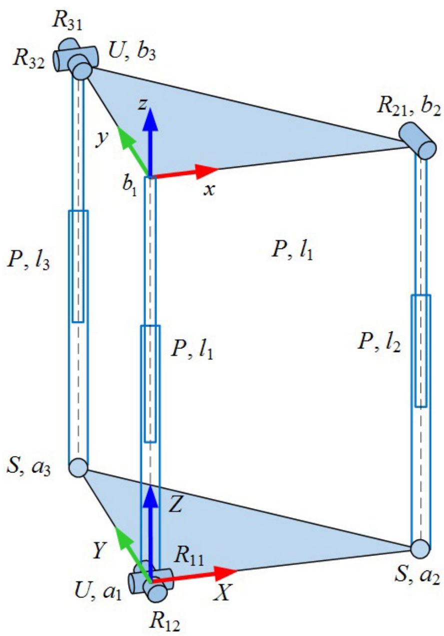

Fig. 4. Sketch of the UP+SPR+SPU PM.

Let {*B*} be a coordinate a_1-XYZ with a_1 as its origin fixed on *B* at a_1. {*m*} be a coordinate b_1-xyz with b_1 as its origin fixed on m at b_1. The geometric constraints $\{X|a_1a_2,\ Y|a_1a_3,\ Z\perp B,\ x|b_1b_2,\ y|b_1b_3,\ z\perp m,\ R_{11}|X,\ R_{12}\perp R_{11},\ l_1\perp R_{12},\ l_1\perp m,\ R_{21}\parallel y,\ R_{21}\perp l_2,\ R_{31}\mid y,\ R_{31}\perp R_{32},\ R_{32}\perp l_3\}$ are satisfied. Let ${}^B_m\boldsymbol{R}$ denote the rotational matrix of relative {*m*} to {*B*}, *α* and *β* are two Euler angles about corresponding axes, $s_\theta=\sin\theta$, $c_\theta=\cos\theta$, $t_\theta=\tan\theta$, $sec_\theta=\text{secant}\theta$, it leads to

$$ {}^B_m\boldsymbol{R}=\begin{bmatrix} c_\beta & 0 & s_\beta \\ s_\alpha s_\beta & c_\alpha & -s_\alpha c_\beta \\ -c_\alpha s_\beta & s_\alpha & c_\alpha c_\beta \end{bmatrix}. \tag{40} $$

The points a_i (i = 1, 2, 3) in {*B*} can be expressed as follows:

$$ \boldsymbol{a}_1=\begin{bmatrix}0 & 0 & 0\end{bmatrix}^{\mathrm{T}},\ \boldsymbol{a}_2=\begin{bmatrix}E_2 & 0 & 0\end{bmatrix}^{\mathrm{T}},\ \boldsymbol{a}_2=\begin{bmatrix}0 & E_3 & 0\end{bmatrix}^{\mathrm{T}}. \tag{41} $$

The points b_i (i = 1, 2, 3) in {*B*} can be expressed as follows:

$$ {}^m\boldsymbol{b}_1=\begin{bmatrix}0 & 0 & 0\end{bmatrix}^{\mathrm{T}},\ {}^m\boldsymbol{b}_2=\begin{bmatrix}e_2 & 0 & 0\end{bmatrix}^{\mathrm{T}},\ {}^m\boldsymbol{b}_3=\begin{bmatrix}0 & e_3 & 0\end{bmatrix}^{\mathrm{T}} \tag{42} $$

where E_i (*i* = 2, 3) denotes the distance from point a_1 to a_i, e_i (i = 2, 3) is the distance from point b_1 to b_i, the position vectors $\boldsymbol{b}_i$ (*i* = 1, 2, 3) in {*B*} can be expressed as follows:

$$ \boldsymbol{b}_i={}^B_m\boldsymbol{R}\,{}^m\boldsymbol{b}_i+\boldsymbol{b}_1,\boldsymbol{b}_1=\begin{bmatrix}x_{b1}\\ y_{b1}\\ z_{b1}\end{bmatrix}. \tag{43} $$

Based on the structure constraint $l_1\perp m$, it leads to

$$ \begin{aligned} & x_{b1}=l_1s_\beta=\frac{z_{b1}}{c_\alpha c_\beta}s_\beta=\frac{z_{b1}t_\beta}{c_\alpha},\ l_i=\left\|\boldsymbol{b}_i-\boldsymbol{a}_i\right\| \\ & y_{b1}=-l_1s_\alpha c_\beta=-\frac{z_{b1}}{c_\alpha c_\beta}s_\alpha c_\beta=-t_\alpha z_{b1} \\ & z_{b1}=l_1c_\alpha c_\beta,\ l_1=\frac{z_{b1}}{c_\alpha c_\beta}. \end{aligned} \tag{44} $$

5.2 Velocity and acceleration analysis of the UP+SPR+SPU PM

From Eq. (44), the linear velocity $\boldsymbol{v}_{b1}$ of point b_1 relative to a_1 can be expressed as follows:

$$ \begin{aligned} & \boldsymbol{v}_{b1}=\boldsymbol{J}_v\boldsymbol{V}_q,\boldsymbol{V}_q=\begin{bmatrix}\dot\alpha\ \dot\beta\ \dot z_{b1}\end{bmatrix}^T \\ & \boldsymbol{J}_v=\begin{bmatrix} \dfrac{z_{b1}t_\beta t_\alpha}{c_\alpha} & \dfrac{z_{b1}}{c_\alpha}\left(sec_\beta\right)^2 & \dfrac{t_\beta}{c_\alpha} \\ -\left(sec_\alpha\right)^2 z_{b1} & 0 & -t_\alpha \\ 0 & 0 & 1 \end{bmatrix}. \end{aligned} \tag{45} $$

From Eq. (40), the angular velocity of {*m*} relative to {*B*} of the UP+SPR+SPU PM can be expressed as:

$$ \boldsymbol{\omega}={}^o\boldsymbol{J}_\omega\boldsymbol{V}_q,\ {}^o\boldsymbol{J}_\omega=\begin{bmatrix}1 & 0 & 0\\ 0 & c_\alpha & 0\\ 0 & s_\alpha & 0\end{bmatrix}. \tag{46} $$

From Eqs. (42) and (43) it leads to

$$ \boldsymbol{V}=\begin{bmatrix}\boldsymbol{v}_{b1}\\ \boldsymbol{\omega}\end{bmatrix}=\boldsymbol{J}_B\boldsymbol{V}_q,\ \boldsymbol{J}_B=\begin{bmatrix}\boldsymbol{J}_v\\ {}^o\boldsymbol{J}_\omega\end{bmatrix} \tag{47} $$

where, $\boldsymbol{J}_B$ is a 6×3 form velocity decoupling matrix of the UP+SPR+SPU PM.

Differentiating both sides of Eq. (47) to time leads to

$$ \begin{aligned} & \dot{\boldsymbol{V}}=\begin{bmatrix}\boldsymbol{J}_v\\ {}^o\boldsymbol{J}_\omega\end{bmatrix}\begin{bmatrix}\ddot\alpha\\ \ddot\beta\\ \ddot z_{b1}\end{bmatrix}+\begin{bmatrix}\dot\alpha & \dot\beta & \dot z_{b1}\end{bmatrix}\begin{bmatrix}\dot{\boldsymbol{J}}_v\\ {}^o\dot{\boldsymbol{J}}_\omega\end{bmatrix}\begin{bmatrix}\dot\alpha\\ \dot\beta\\ \dot z_{b1}\end{bmatrix} \\ & \dot{\boldsymbol{J}}_v=\begin{bmatrix}{}^o\boldsymbol{J}_{v1}\\ {}^o\boldsymbol{J}_{v2}\\ {}^o\boldsymbol{J}_{v3}\end{bmatrix},\ {}^o\dot{\boldsymbol{J}}_\omega=\begin{bmatrix}{}^o\boldsymbol{J}_{\omega1}\\ {}^o\boldsymbol{J}_{\omega2}\\ {}^o\boldsymbol{J}_{\omega3}\end{bmatrix}. \end{aligned} \tag{48} $$

5.3 Comparison of theoretical model with Adams model

According to the introduction of the improved model and the classical model, the classical/improved inverse dynamics model can be obtained by bringing the classical/improved velocity model into Eq. (39). Therefore, $\boldsymbol{J}_{\omega1}={}^*\boldsymbol{J}_{\omega1}$, $\boldsymbol{J}_{\omega2}={}^*\boldsymbol{J}_{\omega2}$, $\boldsymbol{J}_{\omega3}={}^*\boldsymbol{J}_{\omega3}$, the classical inverse dynamics model of the UP+SPR+SPU PM can be obtained, and when $\boldsymbol{J}_{\omega1}={}^U\boldsymbol{J}_{\omega1}$, $\boldsymbol{J}_{\omega2}={}^{SPR\&SR}\boldsymbol{J}_{\omega2}$, $\boldsymbol{J}_{\omega3}={}^{SPU\&SU}\boldsymbol{J}_{\omega3}$, it will get its improved model. Here, simulation using Adams is carried out to verify the dynamic model, as shown in Fig. 5. Set $E_2=E_3=e_2=e_3=600$ mm, $l_{ci}=$

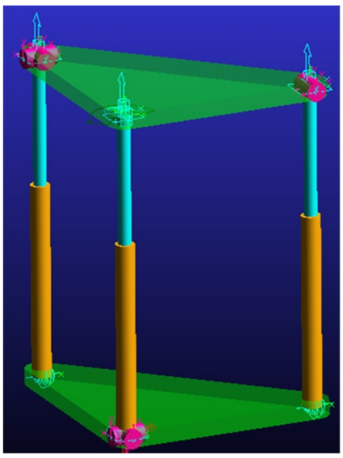

Fig. 5. Simulation manipulator of the UP+SPR+SPU PM in Adams.

l_{pi} = 300 mm (i = 1, 2, 3). Set the mass and inertial parameters as m_o = 26.05 kg, $m_{c1}= m_{c2} = m_{c3}$ = 13.23 kg, $m_{p1} = m_{p2} = m_{p3}$ = 5.88 kg. $\boldsymbol{I}_o$ = diag[1.60 1.19 4.25]×10^6 kg·mm^2, $\boldsymbol{I}_{c1}= \boldsymbol{I}_{c2} = \boldsymbol{I}_{c3}$ = diag[4.00 4.00 0.06]×10^5 kg·mm^2, $\boldsymbol{I}_{p1} = \boldsymbol{I}_{p2} = \boldsymbol{I}_{p3}$ = diag[1.77 1.77 0.01]×10^5 kg·mm^2. Set the independent parameters: z_{b1} = 1000+100cos(0.2πt+0.5π) mm, α = 0.2sin(0.2πt+π)rad, β = 0.2cos(0.2πt+π) rad. The velocity and angular velocity, acceleration and angular acceleration of m can be obtained by bringing the motion parameters into Eqs. (44) and (45), see Fig. 6.

The simulation manipulator through theoretical analysis and simulation, the numerical results of the velocities, accelerations, and driving forces are obtained and shown Figs. 7 and 8, the errors, see Tables 1 and 2, respectively. The mean relative error (E) between the simulated and theoretical data was estimated based on the following equation [30]:

$$E(\%)=\frac{100}{N}\sum_{i=1}^{n}\frac{|simulated\ value - theoretical\ value|}{simulated\ value} . \quad (49)$$

It can be seen from Figs. 7 and 8 that the curve of the improved model and the classical model have similar trends, but different amplitudes. The improved model is closer to the simulated value and has higher accuracy. Among them, the accuracy improvement of kinematics is more significant, while the improvement of dynamics accuracy is relatively small, which may be due to the following two reasons:

Although the accuracy of the kinematic model has been improved, the value of its angular velocity is very small, and the degree of change in the driving force caused by it is limited, so the dynamic accuracy is not improved significantly.

The dynamic model involves many parameters such as structure size, weight, and motion parameters. It is difficult greatly improve the accuracy of the dynamics model by merely improving the accuracy of the angular velocity of the limb.

Table 1. The mean relative errors between the theoretical solution and simulation solution of kinematics.

%E	Theoretical model	l_1	l_2	l_3
ω_i	Classical kinematics	0.8779	0.8753	0.8657
	Improved kinematics	0.1343	0.1324	0.1325
ε_i	Classical kinematics	3.0217	3.0499	3.0801
	Improved kinematics	1.8081	0.3017	0.4061

Table 2. The mean relative errors between the theoretical solution and simulation solution of dynamics.

%E	Theoretical model	l_1	l_2	l_3
F_i	Classical kinematics	2.0350	2.7558	2.6593
	Improved kinematics	2.0285	2.7414	2.6551

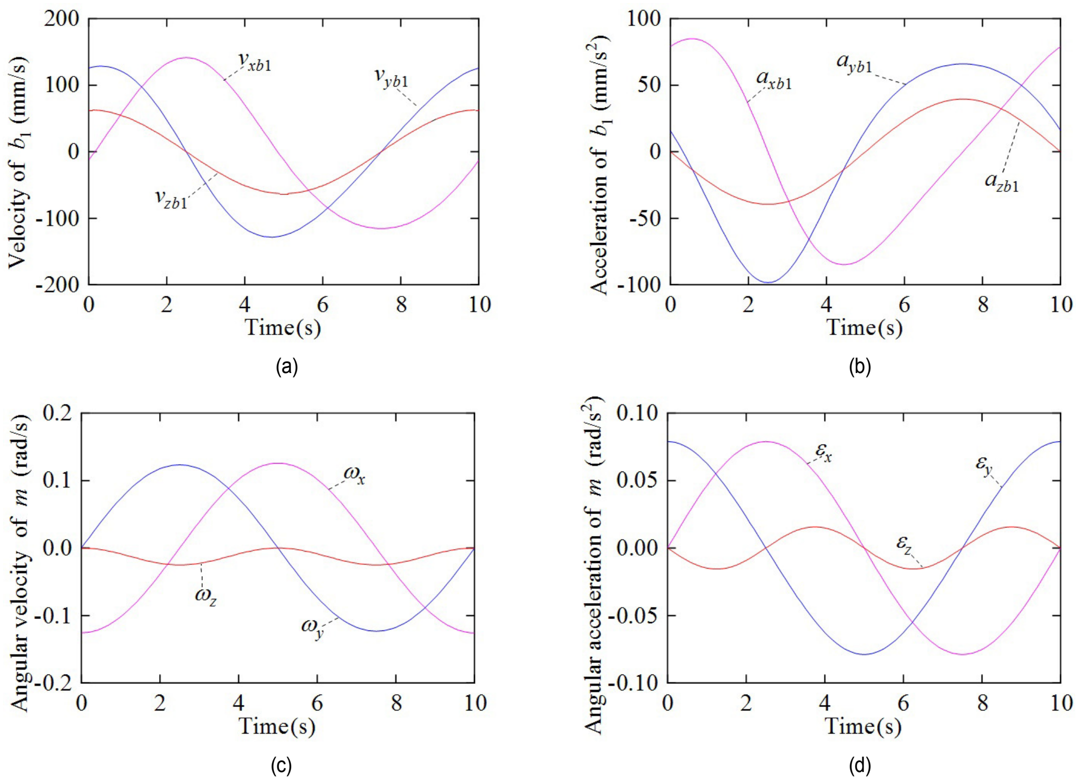

Fig. 6. The translational velocity of m at b_1 (a); translational accelerations (b); the angular velocity of m (c); angular accelerations of m (d).

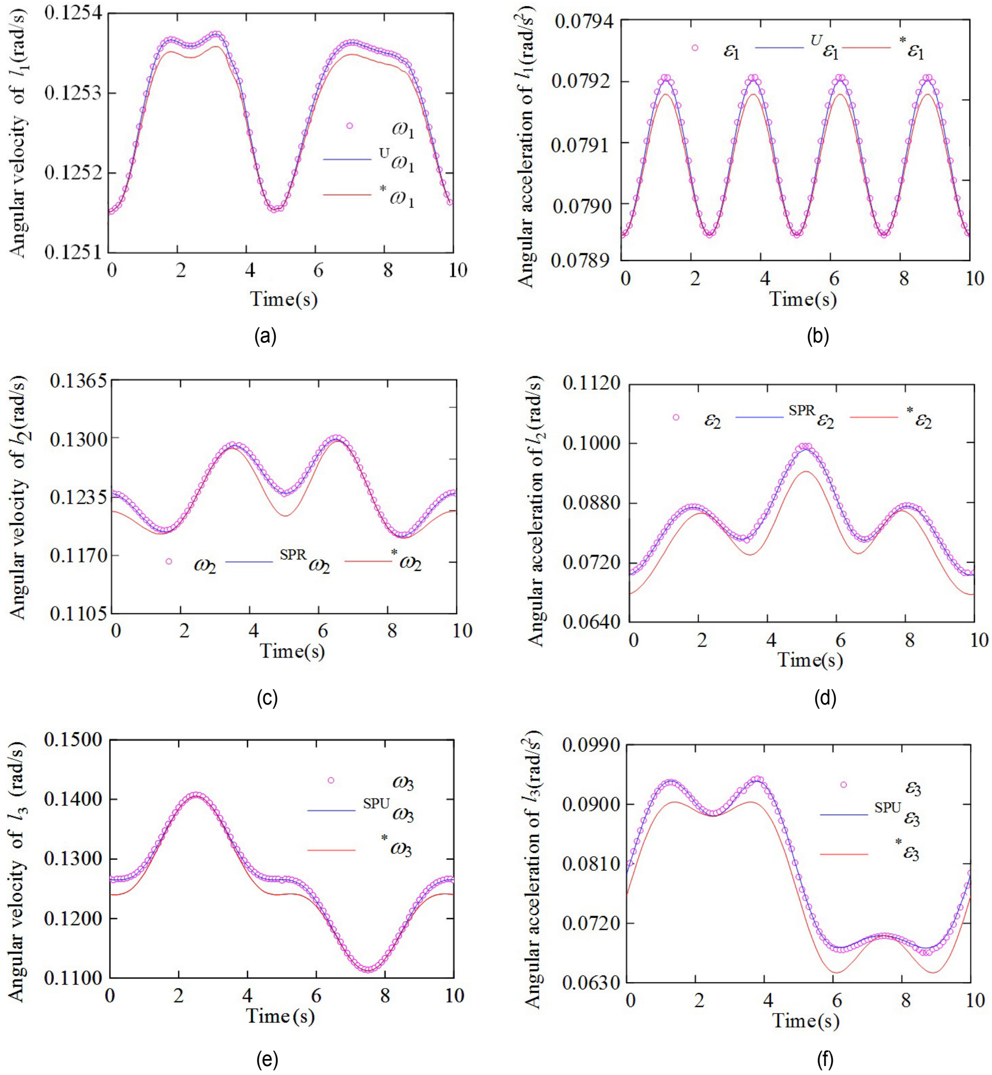

Fig. 7. The angular velocity of UP-type limb l_1 through simulation, improved/classical model (a); angular acceleration of UP-type limb l_1 through simulation, improved/classical model (b); angular velocity of SPR-type limb l_2 through simulation, improved/classical model (c); angular acceleration of SPR-type limb l_2 through simulation, improved/classical model (d); angular velocity of SPU-type limb l_3 through simulation, improved/classical model (e); angular acceleration of SPU-type limb l_3 through simulation, improved/classical model (f).

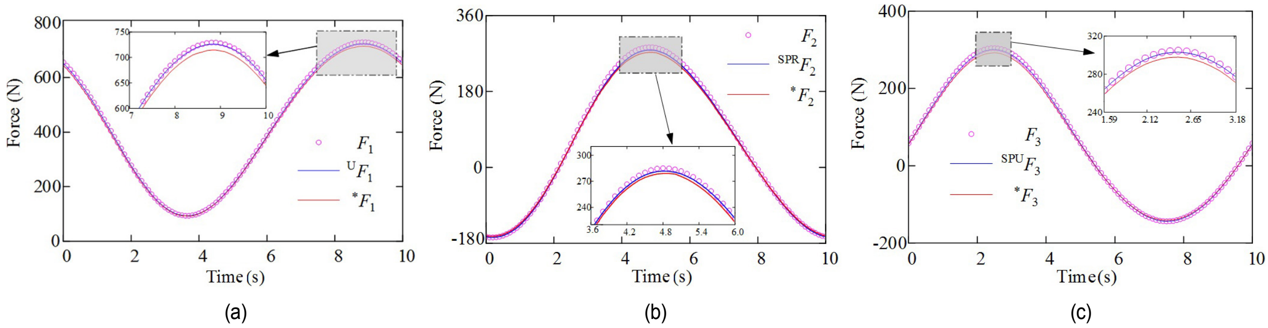

Fig. 8. Numerical comparison of actuation forces between theoretical and Adams results: (a) UP-type limb l_1; (b) SPR-type limb l_2; (c) SPU-type limb l_3.

6. Conclusions

The main contribution of this paper involves the limitations of the classical kinematic model. Compared with previous studies, which only improve the kinematics of the UPS-type limb, this paper establishes the improved angular velocity and angular acceleration models of different limb types (${}^{R}\boldsymbol{\omega}$, ${}^{U}\boldsymbol{\omega}$, ${}^{SPR\&SR}\boldsymbol{\omega}$, ${}^{SPU\&SU}\boldsymbol{\omega}$, ${}^{R}\boldsymbol{\varepsilon}$, ${}^{U}\boldsymbol{\varepsilon}$, ${}^{SPR\&SR}\boldsymbol{\varepsilon}$, ${}^{SPU\&SU}\boldsymbol{\varepsilon}$).

Based on the improved kinematic model, an explicit inverse dynamic model of a general parallel manipulator with clear physical meaning is established.

Taking the 3-DOF UP+SPR+SPU PM simulation results in the Adams software as the standard, the improved model significantly improves on the classical model.

This paper's improved model has a particular reference value for accurately analyzing the kinematics and dynamics of general parallel manipulators of other configurations. At the same time, it lays the foundation for the model modeling of kinematics and dynamics of parallel manipulators with compound limbs and complex configurations.

Acknowledgments

This work was supported by the National Natural Science Foundation of China (U1713219), the European Commission Marie Skodowska-Curie SMOOTH (Smart Robots for Firefighting) Project under Grant H2020-MSCA-RISE-2016-734875, and the Science and Technology (S&T) Program of Hebei under Grant 19211820D and E2020103001, Hebei Natural Science Foundation (E2021203018).

References

[1] B. Dasgupta and T. S. Mruthyunjaya, The Stewart platform manipulator: a review, *Mechanism and Machine Theory*, 35 (1) (2000) 15-40.

[2] J. J. Yu et al., Numeration and type synthesis of 3-DOF orthogonal translational parallel manipulators, *Progress in Natural Science*, 18 (5) (2008) 563-574.

[3] D. Kim and S. H. Hwang, Kinematic Implementation of 3-DOF 2-link type vehicle simulator: Kinematic analysis and motion control method for 3-DOF 2-link type vehicle simulator, *2020 International Conference on Control, Automation and Diagnosis (ICCAD)*, IEEE (2020) 1-6.

[4] R. Aidan, J. Padayachee and G. Bright, Research and development of a 5-axis hybrid kinematic C.N.C. machine, *2017 24th International Conference on Mechatronics and Machine Vision in Practice (M2VIP)*, IEEE (2017) 1-6.

[5] H. A. G. C. Premachandra et al., Genetic algorithm based pick and place sequence optimization for a color and size sorting delta robot, *2020 6th International Conference on Control, Automation and Robotics (ICCAR)*, IEEE (2020) 209-213.

[6] Y. L. Xie et al., Design and analysis of a novel compact XYZ parallel precision positioning stage, *Microsystem Technologies*, 27 (5) (2021) 1925-1932.

[7] S. Wang et al., Type synthesis of rehabilitation mechanism of variable axis bio-fusion knee joint, *J. of Mechanism Engineering*, 56 (11) (2020) 72-79.

[8] J. Y. Niu et al., Kinematic analysis of a serial-parallel hybrid mechanism and its application to a wheel-legged robot, *IEEE Access*, 8 (2020) 111931-111944.

[9] B. Hu et al., Reachable workspace determination for a spatial hyper-redundant manipulator formed by several parallel manipulators, *Journal of Mechanical Science and Technology*, 33 (2) (2019) 869-877.

[10] X. Wu and S. Bai, Analytical determination of shape singularities for three types of parallel manipulators, *Mechanism and Machine Theory*, 149 (2020) 103812.

[11] B. Hu and J. J. Yu, Unified solving inverse dynamics of 6-DOF serial-parallel manipulators, *Applied Mathematical Modelling*, 39 (16) (2015) 4715-4732.

[12] Y. Rong, X. C. Zhang and M. K. Qu, Unified inverse dynamics for a novel class of metamorphic parallel mechanisms, *Applied Mathematical Modelling*, 74 (2019) 280-300.

[13] X. Wang, J. Wu and Y. Wang, Dynamics evaluation of 2UPU/S.P. parallel mechanism for a 5-DOF hybrid robot considering gravity, *Robotics and Autonomous Systems*, 135 (2021) 103675.

[14] Y. Rong et al., Dynamics modeling and drive parameter prediction of a 5-DOF wheel grinding manipulator arm, *China Mechanical Engineering*, 29 (4) (2018) 449-456.

[15] Y. Rong and Z. L. Jin, Dynamic modeling of 3-DOF parallel mechanical leg and peak prediction of servo motor, *Optics and Precision Engineering*, 20 (9) (2012) 1974-1983.

[16] Y. Q. Li et al., Dynamics parameter identification and control of a spherical 2-DOF redundant driven parallel robot system, *China Mechanical Engineering*, 30 (16) (2019) 1967-1975.

[17] B. Dasgupta and T. S. Mruthyunjaya, A newton-euler formulation for the inverse dynamics of the stewart platform manipulator, *Mechanism and Machine Theory*, 33 (8) (1998) 1135-1152.

[18] J. Wang and C. M. Gosselin, A new approach for the dynamic analysis of parallel manipulators, *Multibody System Dynamics*, 2 (3) (1998) 317-334.

[19] G. Cheng and X. L. Shan, Dynamics analysis of a parallel hip joint simulator with four degree of freedoms (3R1T), *Nonlinear Dynamics*, 70 (4) (2012) 2475-2486.

[20] E. F. Fichter, Stewart platform-based manipulator: general theory and practical construction, *International J. of Robotics Research*, 5 (2) (1986) 157-182.

[21] L. W. Tsai, Solving the inverse dynamics of a Stewart-Gough manipulator by the principle of virtual work, *ASME J. of Mechanical Design*, 122 (1) (2000) 3-9.

[22] M. Li et al., Dynamic formulation and performance comparison of the 3-DOF modules of two reconfigurable P.K.M. - the tricept and the trivariant, *ASME J. of Mechanical Design*, 127 (6) (2005) 1129-1136.

[23] S. Briot et al., Degeneracy conditions of the dynamic model of parallel robots, *Multibody System Dynamics*, 37 (4) (2016) 371-412.

[24] C. C. Li et al., An improved inverse dynamics model of 6 D.O.F. motion simulator dynamic, *Acta Armamentarii*, 30 (4) (2009) 446-450.

[25] Z. Q. He et al., Improved newton-euler dynamic models for a Stewart platform, *J. of Vibration and Shock*, 37 (9) (2018) 221-229.

[26] S. Pedrammehr, M. Mahboubkhah and N. Khani, Improved dynamic equations for the generally configured stewart platform manipulator, *Journal of Mechanical Science and Tech-*

nology, 26 (3) (2012) 711-721.
[27] Y. Lu, N. J. Ye and Z. F. Chang, Derivation of general acceleration and hessian matrix of kinematic limbs in parallel manipulator by extended skew-symmetric matrixes, *Archives of Computational Methods in Engineering*, 28 (4) (2021) 3035-3047.
[28] Y. Yu et al., Kinematic analysis and testing of a 6-RRRPRR. parallel manipulator, *Proceedings of the Institution of Mechanical Engineers, Part C: J. of Mechanical Engineering Science*, 231 (13) (2017) 2515-2527.
[29] A. Bayram, Trajectory tracking of a planer parallel manipulator by using computed force control method, *Chinese J. of Mechanical Engineering*, 30 (2) (2017) 449-458.
[30] M. C. Garau et al., Drying of orange skin: Drying kinetics modelling and functional properties, *J. of Food Engineering*, 75 (2) (2006) 288-295.

Appendix

Derivation of some formulas in Secs. 3 and 4 of the article.
Completion equation for Eq. (21):

$$
{}^{U}\boldsymbol{\varepsilon}_i = {}^{U}\dot{\boldsymbol{J}}_{\omega i}\boldsymbol{V} + {}^{U}\boldsymbol{J}_{\omega i}\dot{\boldsymbol{V}},
$$

$$
{}^{U}\dot{\boldsymbol{J}}_{\omega i}=\left(\left[\frac{\left(\boldsymbol{R}_{i1}\boldsymbol{R}_{i2}^{\mathrm{T}}-\boldsymbol{R}_{i2}\boldsymbol{R}_{i1}^{\mathrm{T}}\right)\hat{\boldsymbol{w}}_i^2}{\left(\boldsymbol{R}_{i1}\times\boldsymbol{R}_{i2}\right)\cdot l_i\boldsymbol{w}_i}\right]' \quad \left[-\frac{\left(\boldsymbol{R}_{i1}\boldsymbol{R}_{i2}^{\mathrm{T}}-\boldsymbol{R}_{i2}\boldsymbol{R}_{i1}^{\mathrm{T}}\right)\hat{\boldsymbol{w}}_i^2\hat{\boldsymbol{e}}_i}{\left(\boldsymbol{R}_{i1}\times\boldsymbol{R}_{i2}\right)\cdot l_i\boldsymbol{w}_i}\right]'\right),
$$

$$
\left[\frac{\left(\boldsymbol{R}_{i1}\boldsymbol{R}_{i2}^{\mathrm{T}}-\boldsymbol{R}_{i2}\boldsymbol{R}_{i1}^{\mathrm{T}}\right)\hat{\boldsymbol{w}}_i^2}{\left(\boldsymbol{R}_{i1}\times\boldsymbol{R}_{i2}\right)\cdot l_i\boldsymbol{w}_i}\right]'=\frac{\left(\begin{aligned}&\left[\begin{aligned}&\left(\boldsymbol{R}_{i1}\dot{\boldsymbol{R}}_{i2}^{\mathrm{T}}-\dot{\boldsymbol{R}}_{i2}\boldsymbol{R}_{i1}^{\mathrm{T}}\right)\hat{\boldsymbol{w}}_i^2+\\&\left(\boldsymbol{R}_{i1}\boldsymbol{R}_{i2}^{\mathrm{T}}-\boldsymbol{R}_{i2}\boldsymbol{R}_{i1}^{\mathrm{T}}\right)\left(2\hat{\boldsymbol{w}}_i\left(\widehat{{}^{U}\boldsymbol{\omega}_i\times\boldsymbol{w}_i}\right)\right)\end{aligned}\right]\left[\left(\boldsymbol{R}_{i1}\times\boldsymbol{R}_{i2}\right)\cdot l_i\boldsymbol{w}_i\right]-\\&\left[\left(\boldsymbol{R}_{i1}\boldsymbol{R}_{i2}^{\mathrm{T}}-\boldsymbol{R}_{i2}\boldsymbol{R}_{i1}^{\mathrm{T}}\right)\hat{\boldsymbol{w}}_i^2\right]\left[\begin{aligned}&\left(\boldsymbol{R}_{i1}\times\dot{\boldsymbol{R}}_{i2}\right)\cdot l_i\boldsymbol{w}_i+\\&\left(\boldsymbol{R}_{i1}\times\boldsymbol{R}_{i2}\right)\cdot\left(\boldsymbol{v}+\boldsymbol{\omega}\times\boldsymbol{e}_i\right)\end{aligned}\right]\end{aligned}\right)}{\left(\left(\boldsymbol{R}_{i1}\times\boldsymbol{R}_{i2}\right)\cdot l_i\boldsymbol{w}_i\right)^2},
$$

$$
\left[-\frac{\left(\boldsymbol{R}_{i1}\boldsymbol{R}_{i2}^{\mathrm{T}}-\boldsymbol{R}_{i2}\boldsymbol{R}_{i1}^{\mathrm{T}}\right)\hat{\boldsymbol{w}}_i^2\hat{\boldsymbol{e}}_i}{\left(\boldsymbol{R}_{i1}\times\boldsymbol{R}_{i2}\right)\cdot l_i\boldsymbol{w}_i}\right]'=-\frac{\left(\begin{aligned}&\left[\begin{aligned}&\left(\boldsymbol{R}_{i1}\dot{\boldsymbol{R}}_{i2}^{\mathrm{T}}-\dot{\boldsymbol{R}}_{i2}\boldsymbol{R}_{i1}^{\mathrm{T}}\right)\hat{\boldsymbol{w}}_i^2\hat{\boldsymbol{e}}_i+\\&\left(\boldsymbol{R}_{i1}\boldsymbol{R}_{i2}^{\mathrm{T}}-\boldsymbol{R}_{i2}\boldsymbol{R}_{i1}^{\mathrm{T}}\right)\left(2\hat{\boldsymbol{w}}_i\left(\widehat{{}^{U}\boldsymbol{\omega}_i\times\boldsymbol{w}_i}\right)\right)\hat{\boldsymbol{e}}_i+\\&\left(\boldsymbol{R}_{i1}\boldsymbol{R}_{i2}^{\mathrm{T}}-\boldsymbol{R}_{i2}\boldsymbol{R}_{i1}^{\mathrm{T}}\right)\hat{\boldsymbol{w}}_i^2\left(\widehat{\boldsymbol{\omega}\times\boldsymbol{e}_i}\right)\end{aligned}\right]\left[\left(\boldsymbol{R}_{i1}\times\boldsymbol{R}_{i2}\right)\cdot l_i\boldsymbol{w}_i\right]-\\&\left[\left(\boldsymbol{R}_{i1}\boldsymbol{R}_{i2}^{\mathrm{T}}-\boldsymbol{R}_{i2}\boldsymbol{R}_{i1}^{\mathrm{T}}\right)\hat{\boldsymbol{w}}_i^2\hat{\boldsymbol{e}}_i\right]\left[\begin{aligned}&\left(\boldsymbol{R}_{i1}\times\dot{\boldsymbol{R}}_{i2}\right)\cdot l_i\boldsymbol{w}_i+\\&\left(\boldsymbol{R}_{i1}\times\boldsymbol{R}_{i2}\right)\cdot\left(\boldsymbol{v}+\boldsymbol{\omega}\times\boldsymbol{e}_i\right)\end{aligned}\right]\end{aligned}\right)}{\left(\left(\boldsymbol{R}_{i1}\times\boldsymbol{R}_{i2}\right)\cdot l_i\boldsymbol{w}_i\right)^2}.
$$

Completion equation for Eq. (24)

$$
{}^{SPR\&SR}\boldsymbol{\varepsilon}_i = {}^{SPR\&SR}\dot{\boldsymbol{J}}_{\omega i}\boldsymbol{V} + {}^{SPR\&SR}\boldsymbol{J}_{\omega i}\dot{\boldsymbol{V}},
$$

$$
{}^{SPR\&SR}\dot{\boldsymbol{J}}_{\omega i}=\frac{\begin{bmatrix}\left(\widehat{\boldsymbol{\omega}_i\times\boldsymbol{w}_i}\right)\\ \left(\begin{aligned}&-\left(\widehat{\boldsymbol{\omega}_i\times\boldsymbol{w}_i}\right)\hat{\boldsymbol{e}}_i-\hat{\boldsymbol{w}}_i\left(\widehat{\boldsymbol{\omega}\times\boldsymbol{e}_i}\right)+\\&\dot{l}_i\boldsymbol{w}_i\boldsymbol{w}_i^{T}+l_i\left(\boldsymbol{\omega}_i\times\boldsymbol{w}_i\right)\boldsymbol{w}_i^{\mathrm{T}}+l_i\boldsymbol{w}_i\left(\boldsymbol{\omega}_i\times\boldsymbol{w}_i\right)^{\mathrm{T}}\end{aligned}\right)\end{bmatrix}^{T} l_i-\left[\hat{\boldsymbol{w}}_i \quad -\hat{\boldsymbol{w}}_i\hat{\boldsymbol{e}}_i+l_i\boldsymbol{w}_i\boldsymbol{w}_i^{\mathrm{T}}\right]\dot{l}_i}{l_i^2}.
$$

Completion equation for Eq. (32):

$$
{}^{SPU\&SU}\boldsymbol{\varepsilon}_i = {}^{SPU\&SU}\dot{\boldsymbol{J}}_{\omega i}\boldsymbol{V} + {}^{SPU\&SU}\boldsymbol{J}_{\omega i}\dot{\boldsymbol{V}},
$$

$$
{}^{SPU\&SU}\dot{\boldsymbol{J}}_{\omega i}=\left(\left[\frac{\left(\boldsymbol{R}_{i1}\boldsymbol{R}_{i2}^{\mathrm{T}}-\boldsymbol{R}_{i2}\boldsymbol{R}_{i1}^{\mathrm{T}}\right)\hat{\boldsymbol{w}}_i^2}{\left(\boldsymbol{R}_{i1}\times\boldsymbol{R}_{i2}\right)\cdot l_i\boldsymbol{w}_i}\right]' \quad \left[\frac{-\left(\boldsymbol{R}_{i1}\boldsymbol{R}_{i2}^{\mathrm{T}}-\boldsymbol{R}_{i2}\boldsymbol{R}_{i1}^{\mathrm{T}}\right)\left(l_i\hat{\boldsymbol{w}}_i+\hat{\boldsymbol{w}}_i^2\hat{\boldsymbol{e}}_i\right)}{\left(\boldsymbol{R}_{i1}\times\boldsymbol{R}_{i2}\right)\cdot l_i\boldsymbol{w}_i}+\boldsymbol{E}_{3\times3}\right]'\right).
$$

$$
\left[\frac{\left(\boldsymbol{R}_{i1}\boldsymbol{R}_{i2}^{\mathrm{T}}-\boldsymbol{R}_{i2}\boldsymbol{R}_{i1}^{\mathrm{T}}\right)\hat{\boldsymbol{w}}_i^2}{\left(\boldsymbol{R}_{i1}\times\boldsymbol{R}_{i2}\right)\cdot l_i\boldsymbol{w}_i}\right]'=\frac{\left(\begin{aligned}&\left[\begin{aligned}&\left(\dot{\boldsymbol{R}}_{i1}\boldsymbol{R}_{i2}^{\mathrm{T}}+\boldsymbol{R}_{i1}\dot{\boldsymbol{R}}_{i2}^{\mathrm{T}}-\dot{\boldsymbol{R}}_{i2}\boldsymbol{R}_{i1}^{\mathrm{T}}-\boldsymbol{R}_{i2}\dot{\boldsymbol{R}}_{i1}^{\mathrm{T}}\right)\hat{\boldsymbol{w}}_i^2+\\&\left(\boldsymbol{R}_{i1}\boldsymbol{R}_{i2}^{\mathrm{T}}-\boldsymbol{R}_{i2}\boldsymbol{R}_{i1}^{\mathrm{T}}\right)\left(2\hat{\boldsymbol{w}}_i\left(\widehat{\boldsymbol{\omega}_i\times\boldsymbol{w}_i}\right)\right)\end{aligned}\right]\left[\left(\boldsymbol{R}_{i1}\times\boldsymbol{R}_{i2}\right)\cdot l_i\boldsymbol{w}_i\right]-\\&\left[\left(\boldsymbol{R}_{i1}\boldsymbol{R}_{i2}^{\mathrm{T}}-\boldsymbol{R}_{i2}\boldsymbol{R}_{i1}^{\mathrm{T}}\right)\hat{\boldsymbol{w}}_i^2\right]\left[\begin{aligned}&\left(\boldsymbol{R}_{i1}\times\dot{\boldsymbol{R}}_{i2}\right)\cdot l_i\boldsymbol{w}_i+\\&\left(\boldsymbol{R}_{i1}\times\boldsymbol{R}_{i2}\right)\cdot\left(\boldsymbol{v}+\boldsymbol{\omega}\times\boldsymbol{e}_i\right)\end{aligned}\right]\end{aligned}\right)}{\left(\left(\boldsymbol{R}_{i1}\times\boldsymbol{R}_{i2}\right)\cdot l_i\boldsymbol{w}_i\right)^2},
$$

$$
\left[\frac{-\left(\boldsymbol{R}_{i1}\boldsymbol{R}_{i2}^{\mathrm{T}}-\boldsymbol{R}_{i2}\boldsymbol{R}_{i1}^{\mathrm{T}}\right)\left(l_i\hat{\boldsymbol{w}}_i+\hat{\boldsymbol{w}}_i^2\hat{\boldsymbol{e}}_i\right)}{\left(\boldsymbol{R}_{i1}\times\boldsymbol{R}_{i2}\right)\cdot l_i\boldsymbol{w}_i}+\boldsymbol{E}_{3\times3}\right]'=
$$

$$
-\frac{\left(\begin{aligned}&\left[\begin{aligned}&\left(\dot{\boldsymbol{R}}_{i1}\boldsymbol{R}_{i2}^{\mathrm{T}}+\boldsymbol{R}_{i1}\dot{\boldsymbol{R}}_{i2}^{\mathrm{T}}-\boldsymbol{R}_{i1}\dot{\boldsymbol{R}}_{i2}^{\mathrm{T}}-\dot{\boldsymbol{R}}_{i2}\boldsymbol{R}_{i1}^{\mathrm{T}}\right)\left(l_i\hat{\boldsymbol{w}}_i+\hat{\boldsymbol{w}}_i^2\hat{\boldsymbol{e}}_i\right)+\\&\left(\boldsymbol{R}_{i1}\boldsymbol{R}_{i2}^{\mathrm{T}}-\boldsymbol{R}_{i2}\boldsymbol{R}_{i1}^{\mathrm{T}}\right)\left[\left(\widehat{\boldsymbol{v}+\boldsymbol{\omega}\times\boldsymbol{e}_i}\right)+2\hat{\boldsymbol{w}}_i\left(\widehat{\boldsymbol{\omega}_i\times\boldsymbol{w}_i}\right)\hat{e}_i+\hat{\boldsymbol{w}}_i^2\left(\widehat{\boldsymbol{\omega}\times\boldsymbol{e}_i}\right)\right]\end{aligned}\right]\left[\left(\boldsymbol{R}_{i1}\times\boldsymbol{R}_{i2}\right)\cdot l_i\boldsymbol{w}_i\right]-\\&\left[\left(\boldsymbol{R}_{i1}\boldsymbol{R}_{i2}^{\mathrm{T}}-\boldsymbol{R}_{i2}\boldsymbol{R}_{i1}^{\mathrm{T}}\right)\hat{\boldsymbol{w}}_i^2\hat{\boldsymbol{e}}_i\right]\left[\begin{aligned}&\left(\boldsymbol{R}_{i1}\times\dot{\boldsymbol{R}}_{i2}\right)\cdot l_i\boldsymbol{w}_i+\\&\left(\boldsymbol{R}_{i1}\times\boldsymbol{R}_{i2}\right)\cdot\left(\boldsymbol{v}+\boldsymbol{\omega}\times\boldsymbol{e}_i\right)\end{aligned}\right]\end{aligned}\right)}{\left(\left(\boldsymbol{R}_{i1}\times\boldsymbol{R}_{i2}\right)\cdot l_i\boldsymbol{w}_i\right)^2}.
$$

Completion equation for Eq. (39)

$$
\boldsymbol{F}_q=\boldsymbol{D}\dot{\boldsymbol{V}}+\boldsymbol{H}\boldsymbol{V}+\boldsymbol{G}+\boldsymbol{E},
$$

$$
\boldsymbol{D}=\left(\boldsymbol{J}_D^{-1}\right)^{\mathrm{T}}\boldsymbol{J}_B^{\mathrm{T}}\sum_{i=1}^{n(2\le n\le 6)}\left(\boldsymbol{J}_{ci}^{\mathrm{T}}\boldsymbol{J}_{ci}m_{ci}+\boldsymbol{J}_{pi}^{\mathrm{T}}\boldsymbol{J}_{pi}m_{pi}+\boldsymbol{J}_{\omega i}^{\mathrm{T}}\left(\tilde{\boldsymbol{I}}_{ci}+\tilde{\boldsymbol{I}}_{pi}\right)\boldsymbol{J}_{\omega i}+\boldsymbol{J}_Q\right),
$$

$$
\boldsymbol{H}=\left(\boldsymbol{J}_D^{-1}\right)^{\mathrm{T}}\boldsymbol{J}_B^{T}\sum_{i=1}^{n(2\le n\le 6)}\left(\begin{aligned}&\boldsymbol{J}_{ci}^{\mathrm{T}}\dot{\boldsymbol{J}}_{ci}m_{ci}+\boldsymbol{J}_{pi}^{\mathrm{T}}\dot{\boldsymbol{J}}_{pi}m_{pi}+\boldsymbol{J}_{\omega i}^{\mathrm{T}}\left(\tilde{\boldsymbol{I}}_{ci}+\tilde{\boldsymbol{I}}_{pi}\right)\dot{\boldsymbol{J}}_{\omega i}-\\&\boldsymbol{J}_{\omega i}^{\mathrm{T}}\left(\widehat{\left(\tilde{\boldsymbol{I}}_{si}+\tilde{\boldsymbol{I}}_{ti}\right)\boldsymbol{\omega}_i}\right)\boldsymbol{J}_{\omega i}+\boldsymbol{J}_R\end{aligned}\right),
$$

$$
\boldsymbol{G}=-\left(\boldsymbol{J}_D^{-1}\right)^{\mathrm{T}}\boldsymbol{J}_B^{\mathrm{T}}\sum_{i=1}^{n(2\le n\le 6)}\left(\boldsymbol{J}_{ci}^{\mathrm{T}}m_{ci}\boldsymbol{g}+\boldsymbol{J}_{pi}^{\mathrm{T}}m_{pi}\boldsymbol{g}+\boldsymbol{J}_S\right),
$$

$$
\boldsymbol{E}=-\left(\boldsymbol{J}_D^{-1}\right)^{\mathrm{T}}\boldsymbol{J}_B^{\mathrm{T}}\begin{pmatrix}\boldsymbol{F}\\ \boldsymbol{T}\end{pmatrix},
$$

$$
\boldsymbol{F}_q=\left[F_1,\cdots F_n\right]^{\mathrm{T}}\left(2\le n\le 6\right),
$$

$$
\boldsymbol{J}_{E0}=\left[\boldsymbol{E}_{3\times3}\ \ \boldsymbol{0}_{3\times3}\right],\ \boldsymbol{J}_{0E}=\left[\boldsymbol{0}_{3\times3}\ \ \boldsymbol{E}_{3\times3}\right],
$$

$$
\boldsymbol{J}_{\omega i}=\left\{{}^{*}\boldsymbol{J}_{\omega i},{}^{R}\boldsymbol{J}_{\omega i},{}^{U}\boldsymbol{J}_{\omega i},{}^{SPR\&SR}\boldsymbol{J}_{\omega i},{}^{SPU\&SU}\boldsymbol{J}_{\omega i}\right\},
$$

$$
\dot{\boldsymbol{J}}_{\omega i}=\left\{{}^{*}\dot{\boldsymbol{J}}_{\omega i},{}^{R}\dot{\boldsymbol{J}}_{\omega i},{}^{U}\dot{\boldsymbol{J}}_{\omega i},{}^{SPR\&SR}\dot{\boldsymbol{J}}_{\omega i},{}^{SPU\&SU}\dot{\boldsymbol{J}}_{\omega i}\right\},
$$

$$
\boldsymbol{V}=\left[v_x\ v_y\ v_z\ \omega_x\ \omega_y\ \omega_z\right]^{\mathrm{T}},\dot{\boldsymbol{V}}=\left[a_x\ a_y\ a_z\ \varepsilon_x\ \varepsilon_y\ \varepsilon_z\right]^{\mathrm{T}},
$$

$$
\boldsymbol{J}_Q=\begin{bmatrix}m_o\boldsymbol{E}_{3\times3} & \boldsymbol{0}_{3\times3}\\ \boldsymbol{0}_{3\times3} & \tilde{\boldsymbol{I}}_o\end{bmatrix},\ \boldsymbol{J}_R=\begin{bmatrix}\boldsymbol{0}_{6\times6}\\ -\left(\widehat{\tilde{\boldsymbol{I}}_o\boldsymbol{\omega}}\right)\boldsymbol{J}_{0E}\end{bmatrix},\ \boldsymbol{J}_S=\left[m_o\boldsymbol{g}\ \ 0\ \ 0\ \ 0\right]^{T}.
$$

Completion equation for Eq. (48):

$$
{}^{o}\boldsymbol{J}_{v1}=\begin{bmatrix}\frac{\partial^2 x_{b1}}{\partial\alpha\partial\alpha} & \frac{\partial^2 x_{b1}}{\partial\alpha\partial\beta} & \frac{\partial^2 x_{b1}}{\partial\alpha\partial z_{B1}}\\ \frac{\partial^2 x_{b1}}{\partial\beta\partial\alpha} & \frac{\partial^2 x_{b1}}{\partial\beta\partial\beta} & \frac{\partial^2 x_{b1}}{\partial\beta\partial z_{b1}}\\ \frac{\partial^2 x_{b1}}{\partial z_{b1}\partial\alpha} & \frac{\partial^2 x_{b1}}{\partial z_{b1}\partial\beta} & \frac{\partial^2 x_{b1}}{\partial z_{b1}\partial z_{b1}}\end{bmatrix},\ {}^{o}\boldsymbol{J}_{v2}=\begin{bmatrix}\frac{\partial^2 y_{b1}}{\partial\alpha\partial\alpha} & \frac{\partial^2 y_{b1}}{\partial\alpha\partial\beta} & \frac{\partial^2 y_{b1}}{\partial\alpha\partial z_{b1}}\\ \frac{\partial^2 y_{b1}}{\partial\beta\partial\alpha} & \frac{\partial^2 y_{b1}}{\partial\beta\partial\beta} & \frac{\partial^2 y_{b1}}{\partial\beta\partial z_{b1}}\\ \frac{\partial^2 y_{b1}}{\partial z_{b1}\partial\alpha} & \frac{\partial^2 y_{b1}}{\partial z_{b1}\partial\beta} & \frac{\partial^2 y_{b1}}{\partial z_{b1}\partial z_{b1}}\end{bmatrix},\ {}^{o}\boldsymbol{J}_{v3}=\begin{bmatrix}0&0&0\\0&0&0\\0&0&0\end{bmatrix},
$$

$$
{}^{o}\boldsymbol{J}_{\omega1}=\begin{bmatrix}0&0&0\\0&0&0\\0&0&0\end{bmatrix},\ {}^{o}\boldsymbol{J}_{\omega2}=\begin{bmatrix}0&0&0\\-s_\alpha&0&0\\0&0&0\end{bmatrix},\ {}^{o}\boldsymbol{J}_{\omega3}=\begin{bmatrix}0&0&0\\c_\alpha&0&0\\0&0&0\end{bmatrix},
$$

$$
\frac{\partial^2 x_{b1}}{\partial\alpha\partial\alpha}=z_{b1}t_\beta\left(\frac{\left(sec_\alpha\right)^2c_\alpha+t_\alpha s_\alpha}{\left(c_\alpha\right)^2}\right),\ \frac{\partial^2 x_{b1}}{\partial\alpha\partial\beta}=\frac{\partial^2 x_{b1}}{\partial\beta\partial\alpha}=\frac{z_{b1}t_\alpha}{c_\alpha}\left(sec_\beta\right)^2=\frac{z_{b1}t_\alpha}{c_\alpha\left(c_\beta\right)^2},
$$

$$
\frac{\partial^2 x_{b1}}{\partial\alpha\partial z_{b1}}=\frac{\partial^2 x_{b1}}{\partial z_{b1}\partial\alpha}=\frac{t_\beta t_\alpha}{c_\alpha},\ \frac{\partial^2 x_{b1}}{\partial\beta\partial\beta}=\frac{2z_{b1}sec_\beta\cdot sec_\beta t_\beta}{c_\alpha}=\frac{2z_{b1}\left(sec_\beta\right)^2t_\beta}{c_\alpha},
$$

$$
\frac{\partial^2 x_{b1}}{\partial\beta\partial z_{b1}}=\frac{\partial^2 x_{b1}}{\partial z_{b1}\partial\beta}=\frac{\left(sec_\beta\right)^2}{c_\alpha},\ \frac{\partial^2 x_{b1}}{\partial z_{B1}\partial z_{b1}}=\frac{\partial\frac{t_\beta}{c_\alpha}}{\partial z_{b1}}=0,
$$

$$
\frac{\partial^2 y_{b1}}{\partial\alpha\partial\alpha}=\frac{\partial-\left(sec_\alpha\right)^2z_{b1}}{\partial\alpha}=-2sec_\alpha\cdot sec_\alpha t_\alpha z_{b1}=-2\left(sec_\alpha\right)^2t_\alpha z_{b1},\ \frac{\partial^2 y_{b1}}{\partial\alpha\partial\beta}=\frac{\partial^2 y_{b1}}{\partial\beta\partial\alpha}=\frac{\partial-\left(sec_\alpha\right)^2z_{b1}}{\partial\beta}=0,
$$

$$
\frac{\partial^2 y_{b1}}{\partial\alpha\partial z_{b1}}=\frac{\partial^2 y_{b1}}{\partial z_{b1}\partial\alpha}=\frac{\partial-\left(sec_\alpha\right)^2z_{b1}}{\partial z_{b1}}=-\left(sec_\alpha\right)^2,\ \frac{\partial^2 y_{b1}}{\partial\beta\partial\beta}=\frac{\partial^2 y_{b1}}{\partial\beta\partial z_{b1}}=\frac{\partial^2 y_{b1}}{\partial z_{b1}\partial\beta}=\frac{\partial^2 y_{b1}}{\partial z_{b1}\partial z_{b1}}=0.
$$

Xingchao Zhang received the M.S. in Mechanical Engineering from Hebei Normal University of Science & Technology, China, in 2019. He is currently pursuing the doctorate in Mechatronic Engineering at Yanshan University, China. His main research interests are kinematics and dynamics of parallel robots.

Hongbo Wang received his B.S. and M.S. from Institute of Northeast Heavy Machinery, Qiqihar, China, in 1982 and 1986, respectively. His Ph.D. is from Nagasaki University, Nagasaki, Japan in 1997. Since 2009, he has been with Yanshan University, Qinhuangdao, China as a Professor. His current research interests are in rehabilitation robot and assisting robot for the disabled and the elderly.

Yu Rong has a B.S. in Mechanical Engineering, M.S. and Ph.D. in Mechatronic Engineering from Yanshan University, Qinhuangdao, China, in 2005, 2008, and 2015, respectively. He is currently a lecturer with Yanshan University, China. His research interests include parallel mechanism, robotics.

Jianye Niu received his B.S. in Mechanical Engineering, M.S. and Ph.D. in Mechatronic Engineering from Yanshan University, Qinhuangdao, China, in 2005, 2008, and 2019, respectively. He is currently a postdoctoral researcher with the School of Mechanical Engineering, Hebei University of Technology, Tianjin, China. His research interests include parallel mechanism and its application, rehabilitation robot, mechanical engineering, and artificial neural network.

Junjie Tian received the M.S. in Chemical Process Equipment from Tianjin University, China, in 2018. He is currently pursuing the doctorate in Mechatronic Engineering at Yanshan University, China. His current research interests include rehabilitation robot, robotic compliance control.

Shanshan Li is currently a Ph.D. candidate in Mechanical Engineering, Yanshan University, China. She received her Master's in Mechanical engineering in Hebei Normal University of Science & Technology, China, in 2019. Her current research interests include rehabilitation robot, mechanical engineering.

Yuansheng Ning received the M.S. in Mechanical Engineering from Taiyuan University of Science and Technology, China, in 2020. He is currently pursuing the doctorate in Mechatronic Engineering at Yanshan University, China. His current research interests include rehabilitation robot, robot motion planning and control, robotic compliance control, etc.